RESEARCH ARTICLE

Role of *KEAP1/NRF2* and *TP53* Mutations in Lung Squamous Cell Carcinoma Development and Radiation Resistance

Youngtae Jeong[1,2,3], Ngoc T. Hoang[1,2,4], Alexander Lovejoy[1,2], Henning Stehr[1], Aaron M. Newman[2], Andrew J. Gentles[5,6], William Kong[2], Diana Truong[1,2,7], Shanique Martin[2], Aadel Chaudhuri[3], Diane Heiser[2], Li Zhou[1], Carmen Say[3], Justin N. Carter[3], Susan M. Hiniker[3], Billy W. Loo Jr[1,3], Robert B. West[8], Philip Beachy[2,9,10], Ash A. Alizadeh[11], and Maximilian Diehn[1,2,3]

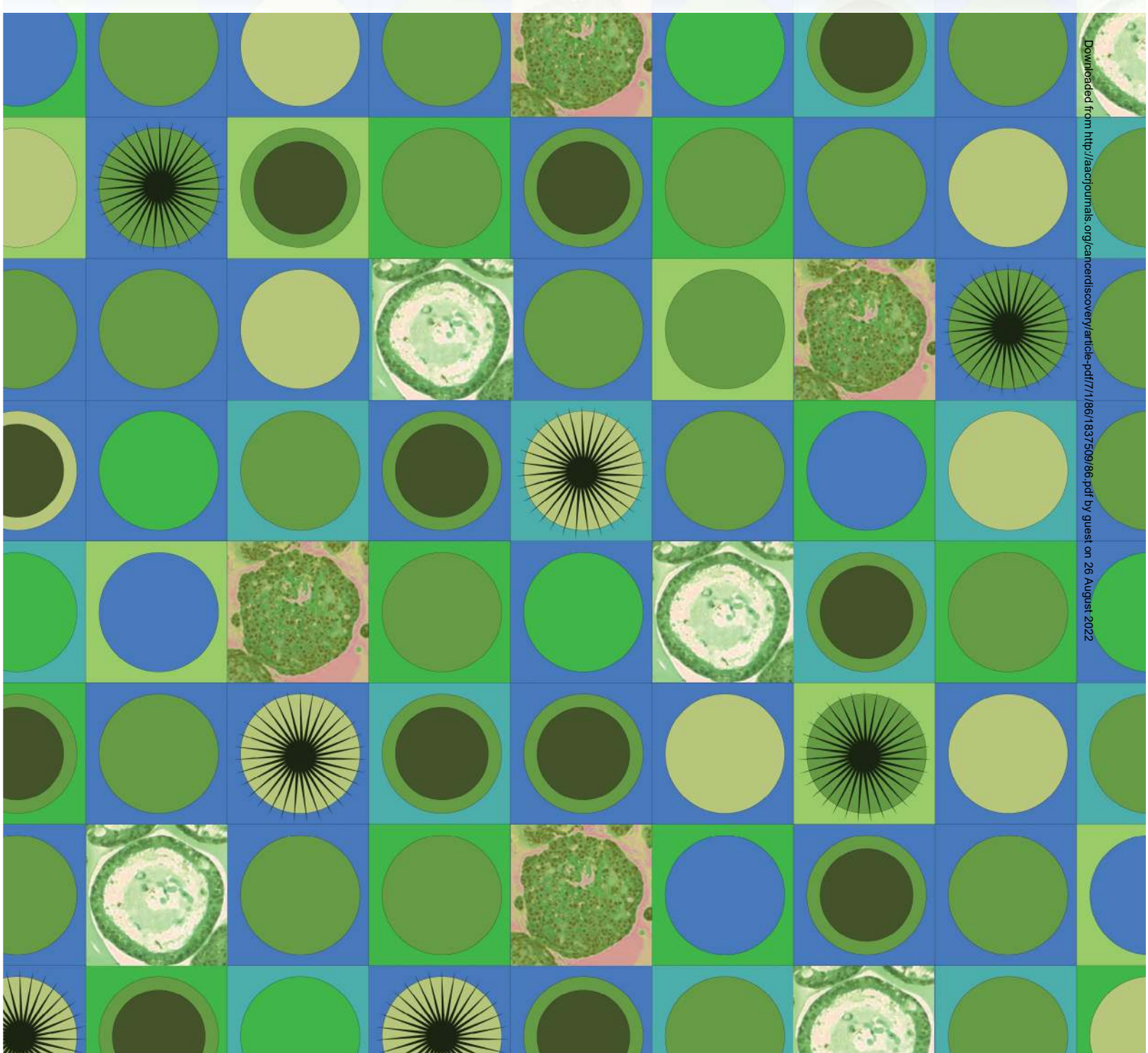

ABSTRACT Lung squamous cell carcinoma (LSCC) pathogenesis remains incompletely understood, and biomarkers predicting treatment response remain lacking. Here, we describe novel murine LSCC models driven by loss of *Trp53* and *Keap1*, both of which are frequently mutated in human LSCCs. Homozygous inactivation of *Keap1* or *Trp53* promoted airway basal stem cell (ABSC) self-renewal, suggesting that mutations in these genes lead to expansion of mutant stem cell clones. Deletion of *Trp53* and *Keap1* in ABSCs, but not more differentiated tracheal cells, produced tumors recapitulating histologic and molecular features of human LSCCs, indicating that they represent the likely cell of origin in this model. Deletion of *Keap1* promoted tumor aggressiveness, metastasis, and resistance to oxidative stress and radiotherapy (RT). *KEAP1/NRF2* mutation status predicted risk of local recurrence after RT in patients with non–small lung cancer (NSCLC) and could be noninvasively identified in circulating tumor DNA. Thus, *KEAP1/NRF2* mutations could serve as predictive biomarkers for personalization of therapeutic strategies for NSCLCs.

SIGNIFICANCE: We developed an LSCC mouse model involving *Trp53* and *Keap1*, which are frequently mutated in human LSCCs. In this model, ABSCs are the cell of origin of these tumors. *KEAP1/NRF2* mutations increase radioresistance and predict local tumor recurrence in radiotherapy patients. Our findings are of potential clinical relevance and could lead to personalized treatment strategies for tumors with *KEAP1/NRF2* mutations. *Cancer Discov; 7(1); 86–101. ©2016 AACR.*

INTRODUCTION

Lung cancer is the second most common cancer in both men and women and the most common cause of cancer death in the United States (1). Lung squamous cell carcinoma (LSCC) comprises a large fraction of non–small cell lung cancers (NSCLC) and annually accounts for 50,000 deaths in the United States. Unlike for lung adenocarcinoma, for which multiple targeted therapies are available, no first-line targeted therapies are currently clinically available for LSCCs. Furthermore, their pathogenesis and cell of origin remain poorly understood, and biomarkers that predict therapeutic responses are lacking. Progress in the field has been slow, in part due to the lack of reliable animal models of LSCCs. Recently, several LSCC mouse models have been reported, involving inactivation of *IKKα*, *Lkb1*, and *Pten* or activation of *Sox2* (2–4). However, a large fraction of mutations that are recurrently found in LSCCs are not included in these studies, and a need remains for the development of additional mouse models of the disease (5).

The Cancer Genome Atlas (TCGA) project has provided a comprehensive landscape of genomic alterations of LSCCs (5). This revealed, as expected, that *TP53* is the most frequently mutated gene, occurring in more than 80% of all LSCCs. In addition to mutations affecting several other pathways, *KEAP1/NRF2* pathway mutations were found in over one third of patients with LSCC. The KEAP1–NRF2 pathway is involved in protection of cells from oxidative and toxic stresses. NRF2 (also known as NFE2L2) is a transcription factor and master regulator of phase II detoxifying and antioxidant genes (6). At homeostasis, NRF2 is bound by the adapter protein KEAP1, which recruits the CUL3 ubiquitin ligase, leading to proteasomal degradation of NRF2 (7, 8). In response to oxidative stress, NRF2 is released from KEAP1, translocates into the nucleus, and promotes the transcription of genes involved in defenses against reactive oxygen species (ROS), such as *GCLM*, *GCLC*, *G6PD2*, and *NQO1*. Recent studies have reported that the KEAP1–NRF2 pathway and levels of ROS contribute to the development and progression of lung cancer (9–13). However, the effects of somatic alterations in *KEAP1/NRF2* and *TP53* on airway stem cells and LSCC tumorigenesis and metastasis have not been deeply explored. Importantly, although a number of groups have examined the effects of KEAP1 and NRF2 on treatment resistance in lung cancer cell lines (14), no studies have done so in genetically engineered mouse models and no studies have demonstrated a clinical association between mutations in *KEAP1/NRF2* and response to radiotherapy in patients with lung cancer.

[1]Stanford Cancer Institute, Stanford University School of Medicine, Stanford, California. [2]Institute for Stem Cell Biology and Regenerative Medicine, Stanford University School of Medicine, Stanford, California. [3]Department of Radiation Oncology, Stanford University School of Medicine, Stanford, California. [4]Department of Biology, San Francisco State University, San Francisco, California. [5]Stanford Center for Cancer Systems Biology, Stanford University School of Medicine, Stanford, California. [6]Department of Radiology, Stanford University School of Medicine, Stanford, California. [7]Department of Biological Sciences, San Jose State University, San Jose, California. [8]Department of Pathology, Stanford University School of Medicine, Stanford, California. [9]Department of Biochemistry, Stanford University School of Medicine, Stanford, California. [10]Howard Hughes Medical Institute, Stanford University School of Medicine, Stanford, California. [11]Division of Oncology, Department of Medicine, Stanford University, Stanford, California.

Note: Supplementary data for this article are available at Cancer Discovery Online (http://cancerdiscovery.aacrjournals.org/).

Corresponding Author: Maximilian Diehn, Stanford University, 875 Blake Wilbur Drive, Stanford, CA 94305-5847. Phone: 650-721-2790; Fax: 650-736-2961; E-mail: diehn@stanford.edu

doi: 10.1158/2159-8290.CD-16-0127

Here, we explore the role of the KEAP1–NRF2 pathway and *Trp53* in the self-renewal of airway basal stem cells (ABSC), LSCC pathogenesis, and prediction of radiation resistance. We found that deletion of *Trp53* or *Keap1* in tracheal epithelial cells promotes ABSC self-renewal. Furthermore, deletion of *Trp53* with or without *Keap1* in tracheal cells leads to the formation of lung cancer with features of squamous cell carcinoma (SCC), whereas the same deletions in peripheral lung cells lead to adenocarcinoma formation. We further demonstrate that ABSCs are the cell of origin for the LSCC in these models. Also, constitutive NRF2 activation and ROS suppression by *Keap1* deletion promoted tumor aggressiveness, metastasis, and resistance to oxidative stress and radiotherapy (RT). Treatment with sulfasalazine, an inhibitor of the antiporter system x_c^-, overcame *Keap1* deletion–mediated radioresistance. Consistently, *KEAP1/NRF2* mutation status in patients with NSCLC was predictive of local recurrence after RT in human patients, and these mutations could be noninvasively identified in circulating tumor DNA (ctDNA). Our findings suggest that system x_c^- is a potential target for personalized radiosensitization of patients with NSCLC harboring *KEAP1/NRF2* mutations and that *KEAP1/NRF2* mutation status is a potential predictive marker for clinical decision making in the treatment of patients with NSCLC.

RESULTS

Inactivation of p53 and KEAP1 Promotes Airway Basal Stem Cell Self-Renewal *In Vitro*

In order to explore the role of mutations in *Keap1* and *Trp53* in LSCC pathogenesis, we began by examining the effects of loss of these genes on the self-renewal of ABSCs, the hypothesized cell of origin for LSCC (15). Bulk tracheal epithelial cells from wild-type (WT) *R26*^{tdTomato}, *Keap1*$^{f/f}$;*R26*^{tdTomato} or *Trp53*$^{f/f}$;*R26*^{tdTomato} mice were transduced with adeno-Cre (Ad-Cre) virus to mimic inactivating mutations of *Keap1* or *Trp53* (Supplementary Fig. S1A and S1B). *In vitro* tracheosphere assays revealed that *Keap1* deletion or silencing increased primary tracheosphere formation by 2- to 3-fold compared with WT cells, consistent with a previous study (ref. 16; Fig. 1A and Supplementary Fig. S1C). To further analyze self-renewal *in vitro*, we dissociated primary tracheospheres into single cells, FACS-sorted tdTomato$^+$ or GFP$^+$ cells, and replated the same number of cells for secondary tracheosphere formation. Secondary tracheosphere formation of *Keap1*-deleted or silenced cells was ~2-fold greater than WT cells (Fig. 1B and Supplementary Fig. S1D). Consistently, upon the single-cell sorting, *Keap1*$^{-/-}$ basal cells from tamoxifen-injected *Krt5*^{CreERT2};*Keap1*$^{f/f}$; *R26*^{tdTomato} mice formed ~70% more tracheospheres than WT basal cells from

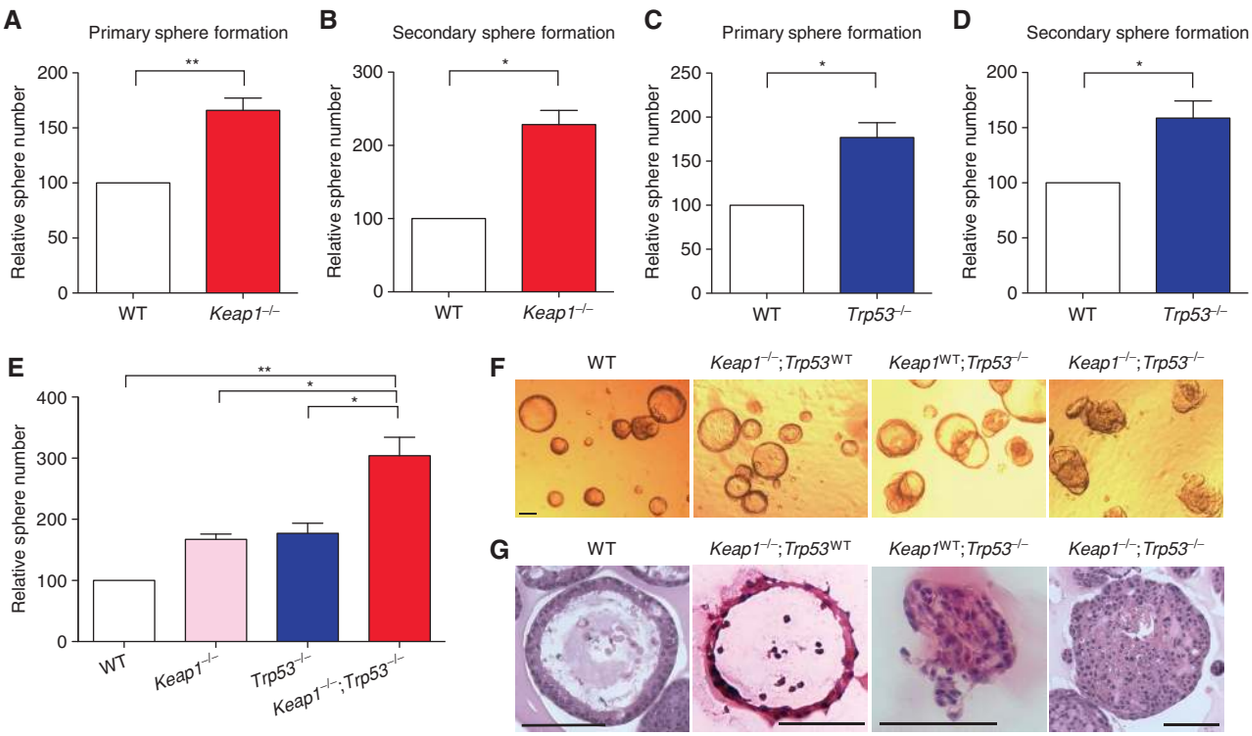

Figure 1. Loss of *Keap1* or *Trp53* promotes airway basal stem cell self-renewal *in vitro*. **A,** Relative number of primary tracheospheres formed by WT or *Keap1*-deleted mouse tracheal epithelial cells ($N = 4$). **B,** Relative number of secondary tracheospheres formed by WT or *Keap1*-deleted cells dissociated from primary tracheospheres ($N = 3$). **C,** Relative number of primary tracheospheres formed by WT or *Trp53*-deleted mouse tracheal epithelial cells ($N = 3$). **D,** Relative number of secondary tracheospheres formed by WT or *Trp53*-deleted cells dissociated from primary tracheospheres ($N = 3$). **E,** Relative number of tracheospheres from WT, *Keap1*$^{-/-}$, *Trp53*$^{-/-}$, and *Keap1*$^{-/-}$;*Trp53*$^{-/-}$ tracheal epithelial cells ($N = 5$ for WT and *Keap1*$^{-/-}$, $N = 3$ for *Trp53*$^{-/-}$, and $N = 4$ for *Keap1*$^{-/-}$;*Trp53*$^{-/-}$). All data in **A–E** are presented as mean ± SEM (*, $P < 0.05$; **, $P < 0.01$). **F,** Brightfield images of tracheospheres initiated by WT, *Keap1*$^{-/-}$, *Trp53*$^{-/-}$, and *Keap1*$^{-/-}$;*Trp53*$^{-/-}$ tracheal epithelial cells. **G,** Hematoxylin and eosin (H&E) staining of WT, *Keap1*$^{-/-}$, *Trp53*$^{-/-}$, and *Keap1*$^{-/-}$;*Trp53*$^{-/-}$ tracheospheres. All scale bars, 100 μm.

tamoxifen-injected *Krt5*^{CreERT2};*R26*^{tdTomato} mice (Supplementary Fig. S1E). Similarly, *Trp53* deletion enhanced primary and secondary tracheosphere formation by 60% to 80% (Fig. 1C and D). These data indicate that inactivation of *Keap1* or *Trp53* promotes ABSC self-renewal *in vitro*.

Because ~80% of LSCCs with mutations in the KEAP1–NRF2 pathway also carry inactivating mutations in *TP53*, we next examined the effects of simultaneous deletion of *Keap1* and *Trp53*. Homozygous deletion of both genes led to an additive increase in tracheosphere number (Fig. 1E). Furthermore, tracheospheres derived from *Keap1*$^{-/-}$;*Trp53*$^{-/-}$ cells displayed aberrant morphologic features manifesting as solid spheres devoid of a central acellular lumen, whereas tracheospheres derived from WT, *Keap1*$^{-/-}$, and *Keap1*$^{f/f}$;*Trp53*$^{f/f}$ cells displayed the expected cystic shape. Tracheospheres derived from *Trp53*$^{-/-}$ cells displayed a mixed phenotype, with a majority of cystic spheres and a minority of compact spheres (Fig. 1F and G and Supplementary Fig. S1F). These data indicate that combined deletion of *Keap1* and *Trp53* leads to greater enhancement of ABSC self-renewal than deletion of either gene alone, and promotes the deregulated expansion of ABSCs.

Inactivation of p53 and KEAP1 Promotes Airway Basal Stem Cell Expansion *In Vivo*

To confirm these findings *in vivo*, we developed a population-based lineage-tracing approach for tracheal epithelial cells. Although intranasal instillation of Ad-Cre induces recombination of peripheral lung cells (17), tracheal epithelial cells are not efficiently transduced, likely due to action of the mucociliary apparatus (Fig. 2A and Supplementary Fig. S2A). We hypothesized that denuding of luminal tracheal cells by SO_2 would allow transduction of tracheal basal cells.

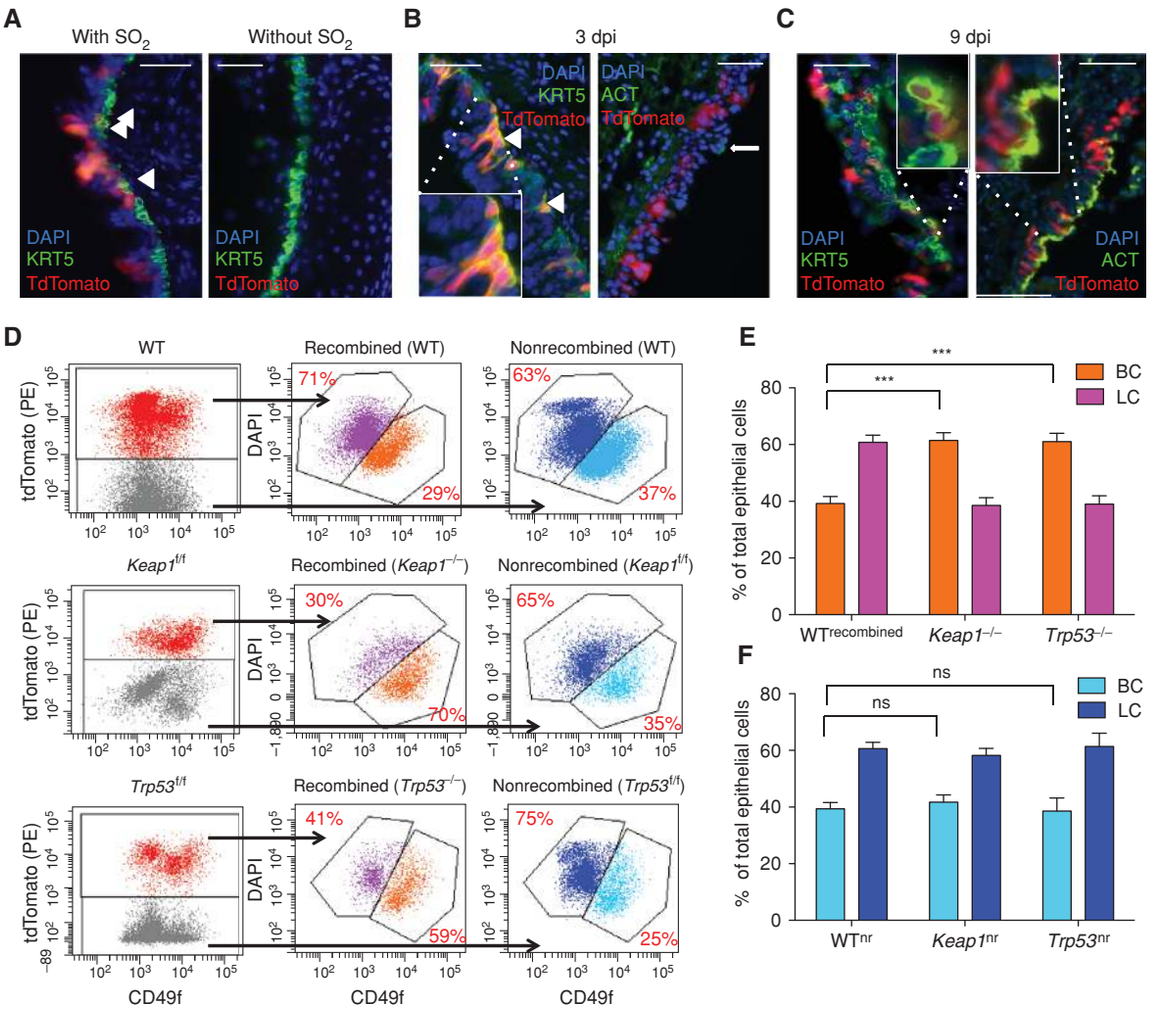

Figure 2. Loss of *Keap1* or *Trp53* promotes airway basal stem cell self-renewal *in vivo*. **A,** *R26*^{tdTomato} mouse trachea 7 days after Ad-Cre transduction with or without preceding SO_2 injury. **B** and **C,** Immunofluorescence staining of tdTomato$^+$ cells (i.e., Ad-Cre–transduced and recombined cells) with basal and luminal markers at 3 and 9 days post-injury (dpi) with Ad-Cre virus intranasally administered at 1 dpi (all scale bars, 100 μm). Tracheae were cut longitudinally and stained for keratin 5 (KRT5) and acetylated tubulin (ACT). **D,** FACS analysis of tracheal basal and luminal cells from *Keap1*^{WT};*Trp53*^{WT};*R26*^{tdTomato}, *Keap1*^{WT};*Trp53*$^{f/f}$;*R26*^{tdTomato}, and *Keap1*$^{f/f}$;*Trp53*^{WT};*R26*^{tdTomato} mice. Ad-Cre viruses were intranasally administered at 20 hours after SO_2 injury, and tracheal cells were harvested at 7 dpi. **E,** Percentage of basal and luminal cells (BC and LC) among recombined cells (red) in **D**. **F,** Percentage of basal and luminal cells among nonrecombined cells (blue) in **D**. All data in **E** and **F** are presented as mean ± SEM ($N = 9$ for WT, $N = 10$ for *Keap1*$^{f/f}$, $N = 5$ for *Trp53*$^{f/f}$; ***, $P < 0.001$). nr, nonrecombined; ns, not significant.

Indeed, Ad-Cre intranasal instillation at 20 hours after SO_2 injury led to recombination in up to 40% of tracheal cells. At 3 days post-injury (dpi), tdTomato$^+$ cells uniformly expressed KRT5 but not acetylated tubulin (ACT), indicating denudation of luminal cells and transduction of basal cells (Fig. 2B). At 9 dpi, however, tdTomato$^+$ cells expressing either KRT5 or ACT were observed, indicating that transduced basal cells had generated luminal cells (Fig. 2C). We used this approach to test if the ratio of basal and luminal tracheal epithelial cells was altered by deletion of *Keap1* or *Trp53*. Specifically, we administered Ad-Cre viruses intranasally to WT *R26*^{tdTomato}, *Keap1*$^{f/f}$;*R26*^{tdTomato}, and *Trp53*$^{f/f}$;*R26*^{tdTomato} immunocompetent mice after SO_2 injury and analyzed the ratio of basal and luminal cells by flow cytometry at 7 dpi. Deletion of either *Keap1* or *Trp53* increased the basal-to-luminal ratio about ~2.5-fold compared with WT or nonrecombined *Keap1*$^{f/f}$ or *Trp53*$^{f/f}$ cells (Fig. 2D–F). In addition, FACS-sorted *Keap1*$^{-/-}$ tdTomato$^+$ cells formed ~3 fold more tracheospheres than WT tdTomato$^+$ cells (Supplementary Fig. S2B). Thus, deletion of *Keap1* or *Trp53* in bulk tracheal epithelial cells leads to expansion of ABSCs *in vivo*.

Development of LSCC from Deletion of *Trp53* with or without *Keap1* in Tracheal Epithelial Cells

These findings prompted us to examine whether deletion of *Trp53* and/or *Keap1* in tracheal epithelial cells leads to LSCC formation. We first attempted to establish tumors *in vivo* using SO_2 injury followed by Ad-Cre intranasal instillation into *Keap1*$^{f/f}$;*Trp53*$^{f/f}$;*R26*^{tdTomato} immunocompetent mice (Fig. 3A). However, as previously observed with *Trp53*$^{f/f}$

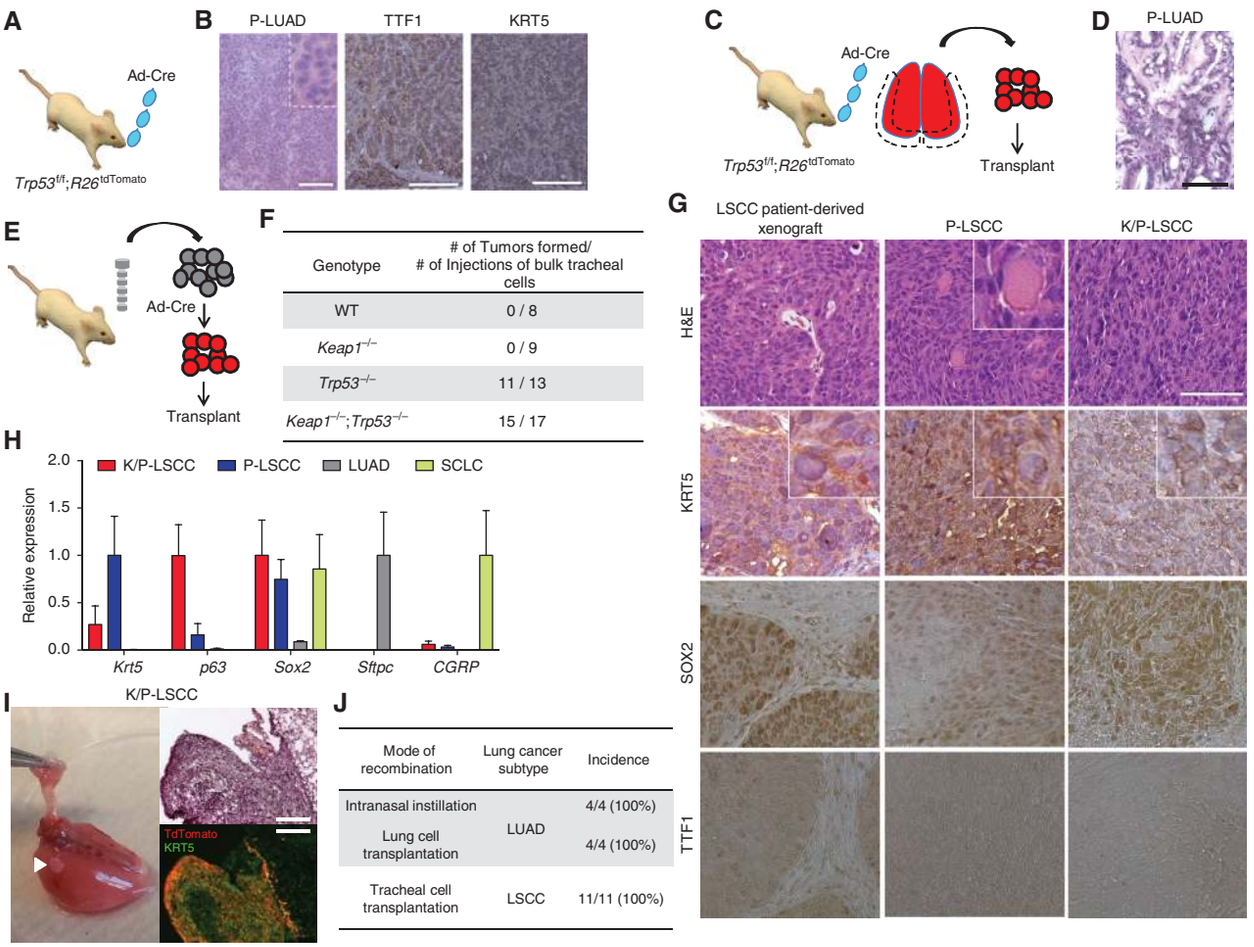

Figure 3. Generation and characterization of LSCCs generated by *Trp53*$^{-/-}$ and *Keap1*$^{-/-}$;*Trp53*$^{-/-}$ tracheal epithelial cells. **A,** Tumor-generating strategy (adenocarcinoma). *Trp53*$^{f/f}$;*R26*^{tdTomato} mice were intranasally instilled with Ad-Cre and observed for tumor formation. **B,** Representative H&E and IHC sections from tumors arising from Ad-Cre–instilled *Trp53*$^{-/-}$ mice in **A**. Expression of TTF1 and KRT5 is shown. P-LUAD, *Trp53*$^{-/-}$ lung adenocarcinoma. **C,** Tumor-generating strategy (adenocarcinoma). tdTomato$^+$ lung cells from Ad-Cre–instilled *Trp53*$^{f/f}$;*R26*^{tdTomato} mice were FACS sorted and transplanted subcutaneously into NOD/SCID IL2Rgamma^{null} (NSG) mice for tumor formation. **D,** Representative H&E-stained sections from tumors arising in NSG mice transplanted with *Trp53*$^{-/-}$ lung cells in (**C**). **E,** Tumor-generating strategy (squamous cell carcinoma). Bulk tracheal epithelial cells (10,000–30,000) were transduced overnight with Ad-Cre viruses *in vitro* and transplanted into NSG mice. **F,** Incidence of tumor formation by WT, *Keap1*$^{-/-}$, *Trp53*$^{-/-}$, and *Keap1*$^{-/-}$;*Trp53*$^{-/-}$ tracheal epithelial cells. **G,** Representative H&E and IHC sections from tumors arising from a human LSCC patient–derived xenograft and K/P- and P-LSCC tumors. Expression of KRT5, SOX2, and TTF1 is shown. **H,** Relative mRNA expression of *Krt5*, *p63*, *Sox2*, *Sftpc*, and *Cgrp* in cells sorted from *Keap1*$^{-/-}$;*Trp53*$^{-/-}$ LSCC (K/P-LSCC), *Trp53*$^{-/-}$ LSCC (P-LSCC), *Kras*^{G12D};*Trp53*$^{-/-}$ LUAD (43), and *Rb*$^{-/-}$;*Trp53*$^{-/-}$;*p130*$^{-/-}$ small cell lung cancer (SCLC; ref. 75; $N = 3$). **I,** Representative gross tumor and stained sections of lung metastases from subcutaneously transplanted K/P-LSCC cells (all scale bars, 100 μm). **J,** Incidence of lung cancer subtypes by different tumor-generating strategies.

mice treated with endotracheal Ad-Cre without SO_2 injury (18), *Trp53*$^{f/f}$;*R26*^{tdTomato} or *Keap1*$^{f/f}$;*Trp53*$^{f/f}$;*R26*^{tdTomato} mice developed SFTPC$^+$NKX2-1$^+$KRT5$^-$ adenocarcinomas in the lung periphery that necessitated euthanasia, regardless of SO_2 injury (Fig. 3B and Supplementary Fig. S3A). No LSCCs were observed, suggesting that the development of adenocarcinomas may not have allowed sufficient time for tumors to emerge in central airways. This observation is consistent with latency times of 8 to 10 months observed in other genetically or chemically induced LSCC models (2, 19, 20). To further test whether *Trp53*-deleted cells in the peripheral lung form lung adenocarcinomas (P-LUAD), we administered Ad-Cre to *Trp53*$^{f/f}$;*R26*^{tdTomato} mice in the absence of SO_2 injury and sorted tdTomato$^+$ epithelial cells from the lung periphery after 1 to 2 weeks. When these cells were transplanted subcutaneously into NOD/SCID IL2Rgamma^{null} (NSG) mice, we observed formation of SFTPC$^+$NKX2-1$^+$KRT5$^-$ adenocarcinomas after ~3 months (Fig. 3C and D and Supplementary Fig. S3B). Finally, when we sorted type II pneumocytes from Ad-Cre transduced *Trp53*$^{f/f}$;*R26*^{tdTomato} mice based on expression of EpCAM and SCA1 (21) and transplanted these into NSG mice, we observed adenocarcinoma formation (data not shown). Thus, deletion of *Trp53* with or without *Keap1* in peripheral lung cells leads to lung adenocarcinoma and not squamous cell carcinoma.

We reasoned that the development of lung adenocarcinoma in these mice may not allow enough time for development of LSCCs. As an alternate strategy, we next treated *Krt5*^{CreERT2};*Keap1*$^{f/f}$;*Trp53*$^{f/f}$;*R26*^{tdTomato} mice with tamoxifen and monitored animals for tumor formation. Unfortunately, these mice developed aggressive skin cancers requiring euthanasia as early as 1 month after treatment due to expression of KRT5 in epidermal basal cells, confounding analysis of LSCC development. Therefore, we next sought to directly test if tracheal cells can give rise to LSCCs. Specifically, we harvested bulk tracheal epithelial cells from WT *R26*^{tdTomato}, *Keap1*$^{f/f}$;*R26*^{tdTomato}, *Trp53*$^{f/f}$;*R26*^{tdTomato}, and *Keap1*$^{f/f}$;*Trp53*$^{f/f}$;*R26*^{tdTomato} tracheae, transduced between 10,000 and 30,000 cells with Ad-Cre overnight, and transplanted these subcutaneously into NSG mice (Fig. 3E). Within 2 to 4 months, tumors appeared in >80% of animals transplanted with either *Trp53*$^{-/-}$ or *Keap1*$^{-/-}$;*Trp53*$^{-/-}$ cells, but never from WT or *Keap1*$^{-/-}$ cells (Fig. 3F). Both *Trp53* and *Keap1* were confirmed to be homozygously deleted in these tumors (Supplementary Fig. S3C). Additionally, these tumors were orthotopically transplantable into lungs (Supplementary Fig. S3D).

Both *Trp53*-deleted (P-LSCC) and *Keap1*/*Trp53*–double-deleted (K/P-LSCC) tumors displayed histologic features of poorly differentiated squamous cell carcinomas, including squamous morphology, nuclear pleomorphism, and dense eosinophilic keratin deposits (Fig. 3G). Consistent with their poorly differentiated histologic appearance, both P-LSCC and K/P-LSCC showed high tumor-initiating cell frequency of ~1/10 in *in vivo*–limiting dilution analyses (Supplementary Table S1). These histologic features were very similar to those observed in patient-derived LSCC xenografts. By immunostaining, K/P- and P-LSCCs, as well as their orthografts, were found to express KRT5, ITGA6, and SOX2, but not TTF1 and SFTPC, again similar to findings from LSCC patient–derived xenografts (Fig. 3G and Supplementary Fig. S3E). Furthermore, K/P-LSCC and P-LSCC tumors expressed high levels of *Krt5, p63*, and *Sox2*, and minimal levels of *Sftpc, Nkx2-1,* and *Cgrp* mRNA (Fig. 3H and Supplementary Fig. S3F). Additionally, compared with WT lung tissue, *Krt5, Krt14*, and *p63* mRNAs were significantly more highly expressed in K/P-LSCCs whereas *Sftpc* expression was negligible (Supplementary Fig. S3G). Additionally, these tumors metastasized to the lung, and the metastatic deposits also expressed KRT5 but not SFTPC (Fig. 3I and Supplementary Fig. S3H and S3I). Thus, whereas deletion of *Trp53* with or without deletion of *Keap1* in peripheral lung cells leads to the formation of tumors closely resembling human LUAD, the same genetic alterations in bulk tracheal epithelial cells lead to formation of tumors closely resembling human LSCC (Fig. 3J).

ABSCs and Not Luminal Tracheal Cells Are the Cell of Origin for LSCC

One of the goals of our study was to identify the cell of origin for LSCC, which has not been experimentally identified, although has been proposed to be central airway basal cells/ABSCs (15). Because LSCCs were initiated from bulk tracheal epithelial cells in our models, we next tested the ability of purified basal or luminal tracheal epithelial cells to give rise to LSCCs, using a similar strategy as previously used in cell-of-origin studies for human and mouse prostate and esophageal cancers (Fig. 4A; refs. 22, 23). First, we sorted tracheal basal and luminal cells from *Keap1*$^{f/f}$;*Trp53*$^{f/f}$;*R26*^{tdTomato} mice, transduced these with Ad-Cre *in vitro*, and transplanted them into NSG mice. Second, we treated *Krt5*^{CreERT2};*Keap1*$^{f/f}$;*Trp53*$^{f/f}$;*R26*^{tdTomato} mice with tamoxifen, allowed ~4 months for luminal cell generation from recombined basal cells, and sorted 500 to 2,000 tdTomato$^+$ tracheal basal and luminal cells for transplantation (Supplementary Fig. S4A). Despite similar cell viability at the time of transplantation (Supplementary Fig. S4B), only basal cells were able to generate tumors, and these displayed similar histologic features as LSCCs arising from bulk tracheal epithelial cells (Fig. 4B and C). Taken together, these data indicate that ABSCs are the likely cell of origin for LSCCs with *TP53* mutation.

Keap1 Loss Contributes to LSCC Pathogenesis via NRF2

Because both *Trp53*- and *Trp53;Keap1*-deleted tracheal cells generated LSCCs, we next sought to examine the role of *Keap1* loss in LSCC pathogenesis by comparing the two types of tumors. Compared with P-LSCC cells, K/P-LSCC cells proliferated more rapidly *in vitro* (Fig. 5A). Similarly, *in vivo* tumor growth studies revealed that K/P-LSCCs grew significantly more rapidly than P-LSCCs when equal numbers of tumor cells were implanted subcutaneously (Fig. 5B). In addition, K/P-LSCC cells displayed significantly higher migratory potential *in vitro* (Fig. 5C) and significantly higher numbers of lung metastases *in vivo* when injected into the tail vein (Fig. 5D).

We next investigated the genome-wide gene expression changes induced by *Keap1* loss by FACS-sorting tumor cells and performing RNA sequencing (RNA-seq). Unsupervised hierarchical clustering of global gene expression profiles displayed concordance between paired replicates and revealed significant differences between the two types of tumors (Supplementary

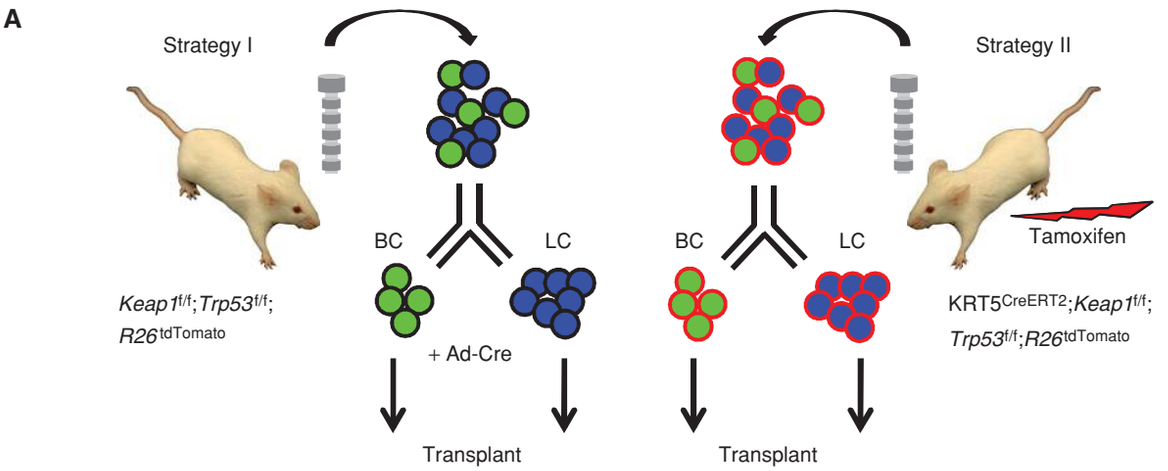

B

	Basal cells	Luminal cells
In vitro recombination	1/3	0/3
In vivo recombination	4/5	0/5
Total	5/8	0/8

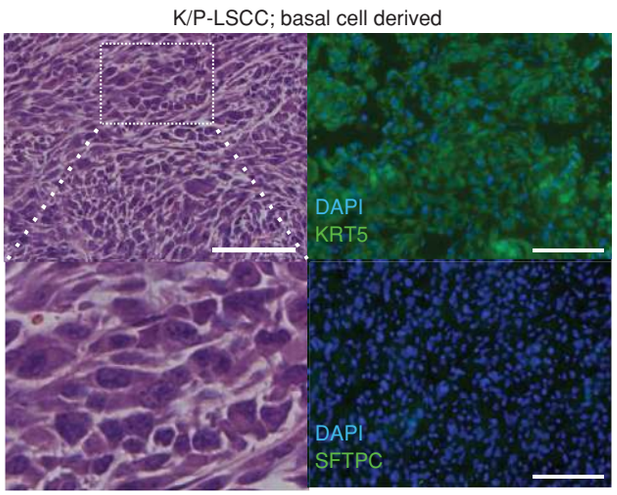

Figure 4. ABSCs are the cell of origin for *Trp53*$^{-/-}$ and *Keap1*$^{-/-}$;*Trp53*$^{-/-}$ LSCCs. **A,** Tumor-generating strategies for the cell-of-origin study (LSCC). For *in vitro* recombination, 10,000 to 30,000 basal cells (BC) and luminal cells (LC) sorted from *Keap1*$^{f/f}$;*Trp53*$^{f/f}$;*R26*^{tdTomato} mice were transduced overnight with Ad-Cre and transplanted subcutaneously into NSG mice. For *in vivo* recombination, 500 to 2,000 basal cells and luminal cells were sorted from Krt5^{CreERT2};*Keap1*$^{f/f}$;*Trp53*$^{f/f}$;*R26*^{tdTomato} mice ~4 months after tamoxifen injection for tumor generation from recombined basal cells and transplanted directly after sorting. **B,** Incidence of tumor formation by tracheal basal cells or luminal cells. **C,** H&E and immunostaining of a tumor arising from sorted luminal cells. All scale bars, 100 μm.

Fig. S5A). Using a 2-fold cutoff and corrected *P*-value threshold < 0.01, 298 genes were upregulated and 463 genes were downregulated in K/P-LSCCs compared with P-LSCCs. Using gene set enrichment analyses (GSEA; ref. 24), we found that K/P-LSCCs overexpressed genes upregulated in stem cells, consistent with our findings in Figs. 1 and 2, showing that *Keap1* deletion enhances ABSC self-renewal (Fig. 5E). In addition, K/P-LSCCs overexpressed gene sets related to NRF2 target genes, phase II conjugation, and biological oxidation. In agreement with these gene expression changes, intracellular ROS levels were significantly lower in K/P-LSCC cells than in P-LSCC cells (Fig. 5F and G).

Previous studies have shown that both NRF2 and NF-κB signaling can serve as downstream mediators of *Keap1* loss (3, 25, 26). Although NRF2 target genes were upregulated by KEAP1 loss, NF-κB target genes were not differentially enriched in either K/P-LSCC or P-LSCC cells (Fig. 5E). Consistently, the expression of selected NF-κB target genes measured by qRT-PCR was not higher in K/P-LSCC compared with P-LSCC cells (Fig. 5H), whereas the expression of NRF2 target genes was significantly increased (Fig. 5I). Furthermore, *Nrf2* silencing in K/P-LSCC cells decreased cell proliferation *in vitro* and tumor growth *in vivo* to levels similar to those seen in P-LSCC cells (Fig. 5J and K and Supplementary Fig. S5B), suggesting that the increased proliferation seen in K/P-LSCCs is largely mediated via NRF2. Also, NOTCH1 target genes, which were previously shown as a downstream mediator NRF2 (16), were not differentially expressed in either of two tumor types (Fig. 5L). These data indicate that loss of *Keap1* in LSCCs leads to increased cell proliferation, invasion, and expression of NRF2 target genes and suggest that NRF2 activation and subsequent ROS decrease is the main mechanistic mediator of phenotypes observed upon *Keap1* loss.

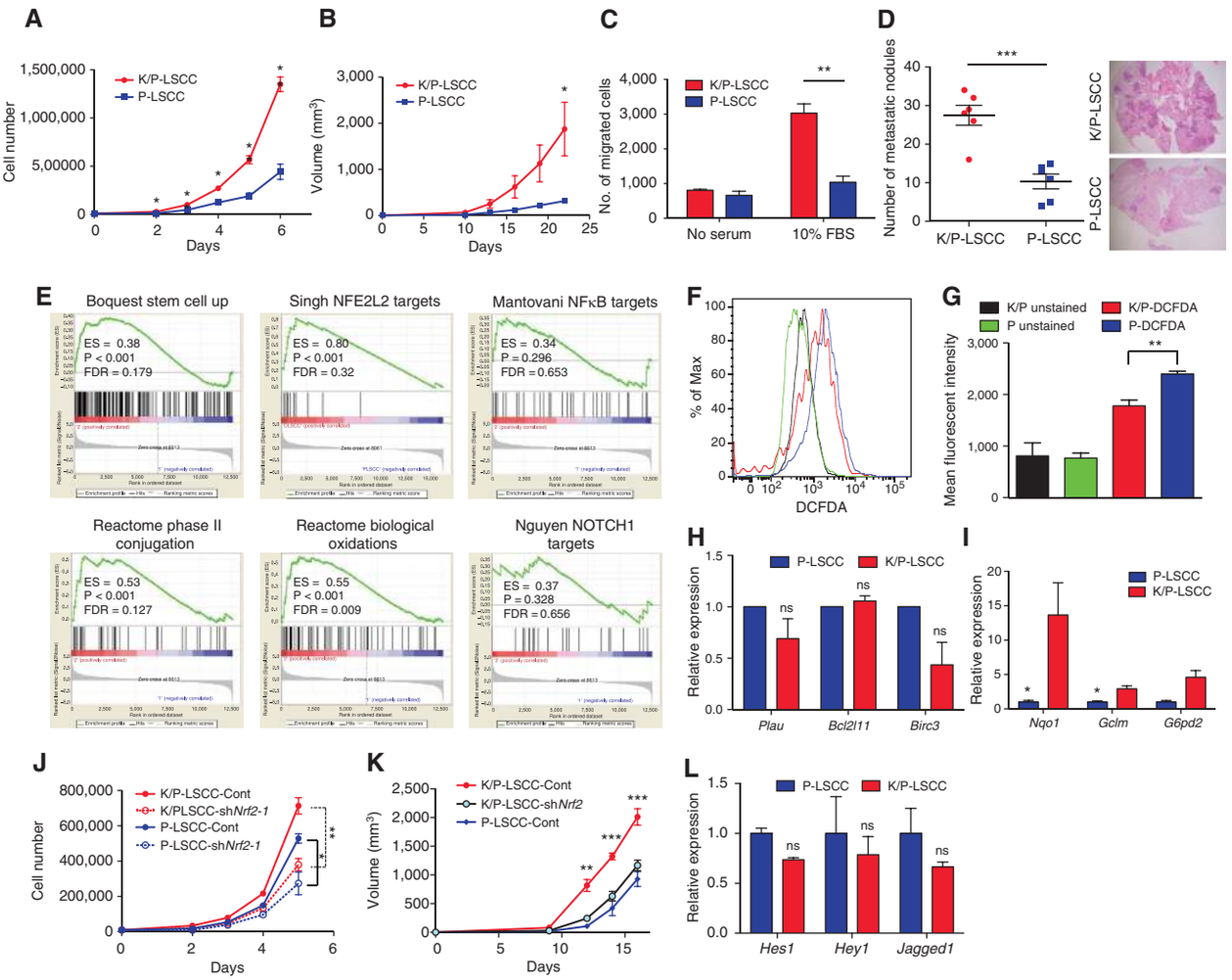

Figure 5. Loss of *Keap1* contributes to LSCC pathogenesis by activating the NRF2–ROS pathway. **A,** *In vitro* cell proliferation of K/P-LSCC and P-LSCC cells ($N = 3$). **B,** *In vivo* tumor growth of K/P-LSCC and P-LSCC tumors ($N = 8$). **C,** *In vitro* cell invasion of K/P-LSCC and P-LSCC cells ($N = 3$). **D,** *In vivo* lung metastasis of K/P-LSCC and P-LSCC cells ($N = 6$). Microscopic metastatic foci in the lung were counted. **E,** Enrichment plots for highly enriched gene sets from GSEA of RNA-seq data (Supplementary Fig. S5A). Gene sets related to stem cells, ROS biology, NF-κB, and Notch are shown. **F** and **G,** FACS analysis (**F**) and bar graph (**G**) of intracellular ROS levels of K/P-LSCC and P-LSCC cells. ROS levels were measured by DCFDA staining. **H,** Expression of NF-κB target genes in K/P-LSCC and P-LSCC cells assayed by qRT-PCR ($N = 3$). **I,** Expression of NRF2 target genes in K/P-LSCC and P-LSCC cells ($N = 3$). **J,** *In vitro* cell proliferation of K/P-LSCC and P-LSCC cells transduced with control or sh*Nrf2* lentivirus ($N = 3$). **K,** *In vivo* growth of K/P-LSCC and P-LSCC tumors with and without sh*Nrf2* lentivirus transduction ($N = 6$). **L,** expression of Notch1 target genes in K/P-LSCC and P-LSCC cells ($N = 3$). All data from **A–D** and **G–L** are presented as mean ± SEM (*, $P < 0.05$; **, $P < 0.01$; ***, $P < 0.001$).

Lowering ROS Mimics Effects of *Keap1* Deletion

To establish the functional relevance of differences in ROS levels observed between P-LSCC and K/P-LSCC cells, we examined whether inhibition of ROS could mimic the effect of *Keap1* loss on LSCC proliferation. Consistent with baseline differences in ROS, treatment with the ROS inhibitor N-Acetylcysteine (NAC) increased tumorsphere formation in P-LSCC but not in K/P-LSCC cells (Fig. 6A and Supplementary Fig. S6A). Next, we asked whether treatment with NAC could mimic the prometastatic effects of *Keap1* deletion. NAC treatment significantly increased the number of metastatic lung nodules formed by P-LSCC cells after tail-vein injection (Fig. 6B and Supplementary Fig. S6B and S6C). Thus, effects of *Keap1* deletion on cell proliferation, clonogenicity, and metastasis can be mimicked by reduction of cellular ROS.

Keap1 Deletion Induces Resistance to Oxidative Stress and Ionizing Radiation

Lower ROS levels induced by *Keap1* deletion should protect K/P-LSCC from oxidative stress. Congruent with this hypothesis, we found that K/P-LSCC cells were significantly more resistant to H_2O_2 treatment than P-LSCC cells (Fig. 6C and Supplementary Fig. S6D). Because the main mechanism of ionizing radiation (IR)–induced cell killing involves DNA damage caused by ROS induction (27), we next explored the effect of *Keap1* deletion on LSCC radiosensitivity. In agreement with our findings of enhanced ability to survive ROS stress, K/P-LSCC cells were significantly more radioresistant than P-LSCC cells in tumorsphere clonogenic assays (Fig. 6D and E). This effect was not unique to our LSCC models, because *Keap1/Trp53*-deleted LUAD (K/P-LUAD) cells

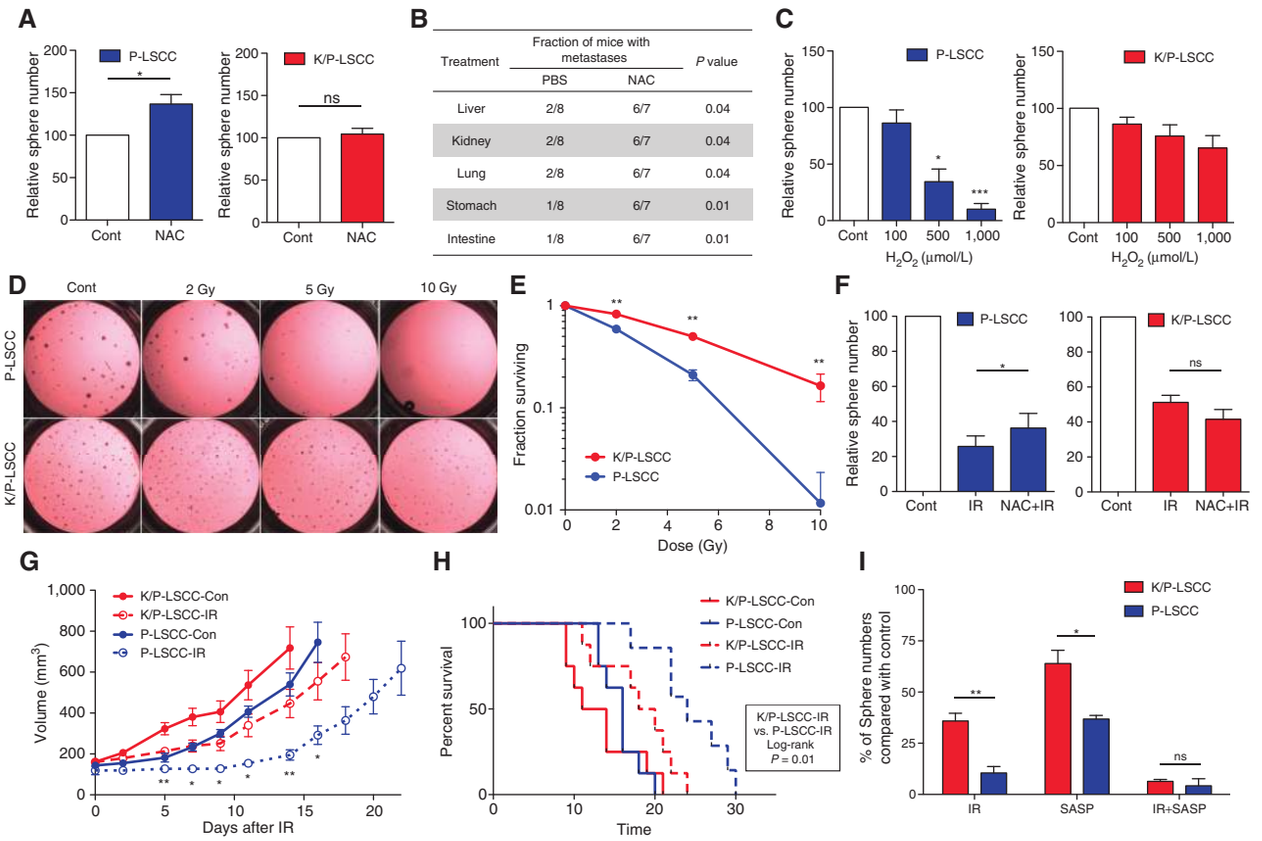

Figure 6. The KEAP1–NRF2 pathway confers LSCC resistance to oxidative stress and irradiation. **A,** Relative number of P-LSCC and K/P-LSCC tumorspheres treated with vehicle (cont) or N-acetylcysteine (NAC; 1 mmol/L) treatment ($N = 4$). **B,** *In vivo* metastasis of P-LSCC cells treated with PBS or NAC (500 μmol/L; $N = 7$–8). **C,** Relative number of P-LSCC and K/P-LSCC tumorspheres treated with 0, 100, 500, and 1,000 μmol/L H_2O_2 treatment ($N = 5$). **D,** Brightfield images of tumorspheres of K/P-LSCCs and P-LSCCs treated with varying doses of ionizing irradiation. **E,** Clonogenic survival of K/P-LSCC and P-LSCC cells treated with varying doses of ionizing radiation ($N = 3$). **F,** Relative number of tumorspheres formed by P-LSCC cells pretreated with vehicle or NAC (500 μmol/L) for 2 hours and then irradiated (5 Gy; $N = 4$). **G,** *In vivo* tumor growth curve of K/P-LSCC and P-LSCC tumors with or without irradiation (6 Gy × 1; $N = 8$). Irradiated K/P-LSCCs and P-LSCCs were compared for tumor growth. **H,** Kaplan–Meier survival curves of K/P-LSCC and P-LSCC tumor–bearing mice ($N = 7$–8). Tumors were irradiated after reaching ~120 mm^3. **I,** Relative number of P-LSCC and K/P-LSCC tumorspheres with irradiation (5 Gy) and/or sulfasalazine (SASP; 100 μmol/L) treatment ($N = 3$). All data in **A–I** are presented as mean ± SEM (*, $P < 0.05$; **, $P < 0.01$; ***, $P < 0.001$).

were also significantly more radioresistant than LUAD cells in which only *Trp53* was deleted (P-LUAD; Supplementary Fig. S7A and S7B). Furthermore, IR-induced phosphorylated histone 2AX (γ-H2AX) nuclear foci were significantly fewer in K/P-LSCC cells than in P-LSCC cells, indicating that K/P-LSCC cells develop less DNA double-strand breaks after IR (Supplementary Fig. S7C and S7D). Additionally, NAC pretreatment significantly protected P-LSCC cells from IR while having no effect on K/P-LSCC cells, consistent with the hypothesis that radioresistance induced by *Keap1* loss is largely mediated through reduction of intracellular ROS (Fig. 6F and Supplementary Fig. S7E). Similarly, *in vivo* growth of K/P-LSCC tumors was significantly less inhibited by IR than that of P-LSCC tumors (Fig. 6G). Also, animals bearing K/P-LSCC tumors showed significantly worse overall survival after *in vivo* irradiation than littermates bearing P-LSCC tumors (Fig. 6H). These data indicate that activation of the KEAP1–NRF2 pathway induces radioresistance in NSCLCs.

Finally, we sought to identify a potential strategy for overcoming *Keap1*-mediated radioresistance. One of the genes most highly overexpressed by K/P-LSCCs compared with P-LSCCs was *Slc7a11* (>15-fold; Supplementary Fig. S8A), which encodes the light chain of the system x_c^- antiporter that plays a critical role in glutathione synthesis via cystine import (28). Therefore, we reasoned that inhibition of system x_c^- may overcome the radioresistant phenotype of K/P-LSCC tumors. Treatment with sulfasalazine, a system x_c^- inhibitor (29–31), in combination with IR, sensitized K/P-LSCCs and resulted in similar cell killing as in P-LSCCs (Fig. 6I and Supplementary Fig. S8B). These data suggest that targeting system x_c^- represents a potential strategy for overcoming *Keap1*-mediated radioresistance.

KEAP1/NRF2 Mutation Status Is a Strong Predictor of RT Outcome in Patients with NSCLC

Based on the findings that both K/P-LSCCs and K/P-LUADs are more radioresistant to IR than P-LSCCs and P-LUADs, respectively, we hypothesized that *KEAP1/NRF2* mutations lead to increased rates of local recurrence in patients with localized NSCLCs treated with RT. We

therefore genotyped a cohort of 42 tumors from patients with stage I–III NSCLC treated with RT, with or without concurrent chemotherapy, and identified 9 patients with mutations in *NRF2* or *KEAP1* (Fig. 7A and Supplementary Table S2). All seven *KEAP1* mutations are predicted to be deleterious to protein structure/function and six are located in the Kelch repeat domain that mediates interaction with NRF2 (Supplementary Table S3). Strikingly, the cumulative incidence of local failure at 30 months was 70% in patients whose tumors carried mutations in *KEAP1/NRF2* and 18% in patients with WT tumors ($P < 0.008$; Fig. 7B). Additionally, out of 12 total patients who developed local recurrence, 6 had tumors with *KEAP1/NRF2* mutations, implicating the pathway in half of RT failures in our cohort. Restricting analysis to patients with stage II–III NSCLC also revealed significantly higher rates of local failure in patients with *KEAP1* or *NRF2* mutations ($P < 0.04$; Fig. 7C). Of note, mutations in *TP53*, which were found in 19 patients, were not associated with risk of local recurrence (Supplementary Fig. S9).

Because patients with NSCLC receiving radiotherapy often undergo only limited tumor tissue sampling via needle biopsies and can therefore have insufficient tissue for mutation testing (32), it would be advantageous to be able to evaluate *KEAP1/NRF2* mutation status noninvasively. To facilitate such analyses, our group developed an ultrasensitive approach for detection of mutant ctDNA called CAPP-Seq (33), which we have recently optimized for noninvasive mutation detection (34). We were able to obtain pretreatment plasma for 7 of the patients in our initial cohort and found that CAPP-Seq analysis correctly identified *KEAP1* mutation status in all of them (Fig. 7D). Furthermore, in 1 patient for whom we analyzed serial plasma samples, the *KEAP1* mutation as well as other co-occurring mutations tracked with treatment response (Fig. 7E).

Finally, in order to test the association of *KEAP1* mutation status with local recurrence after RT in an independent cohort, we analyzed 20 patients for whom we did not have access to tumor tissue. We applied CAPP-Seq to noninvasively genotype each patient's tumor using the pre-RT plasma sample and identified 5 patients with *KEAP1* mutations (Supplementary Table S4). As in our initial cohort, the cumulative incidence of local recurrence was significantly higher in patients with *KEAP1* mutations ($P = 0.02$; Fig. 7F). Taken together, these

A

		Wild-type ($n = 33$)	*KEAP1/NRF2* mutant ($n = 9$)	*P*
Sex	M	9 (27%)	5 (56%)	0.23
	F	24 (73%)	4 (44%)	
Median age, years (range)		70 (42–91)	66 (56–91)	0.45
Median follow-up, mo. (range)		24 (6–53)	25 (7–63)	0.47
Histology	SCC	5 (15%)	1 (11%)	0.85
	Adenoca	25 (76%)	7 (78%)	
	Other	3 (9%)	1 (11%)	
Stage	I	22 (67%)	5 (56%)	0.54
	II	6 (18%)	1 (11%)	
	III	5 (15%)	3 (33%)	
Median tumor volume, mL (range)		16.2 (0.8–569.8)	16.1 (1.0–218.5)	0.48
Radiation type	SABR	25 (76%)	6 (67%)	0.68
	CFRT	8 (24%)	3 (33%)	
Chemotherapy	Yes	7 (21%)	3 (33%)	0.66
	No	26 (79%)	6 (67%)	

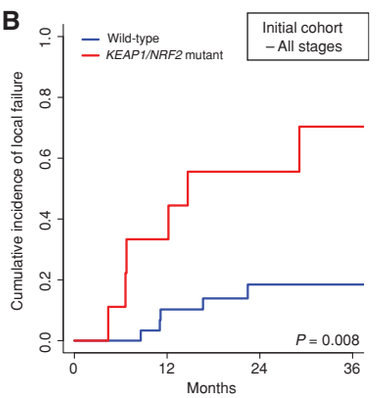

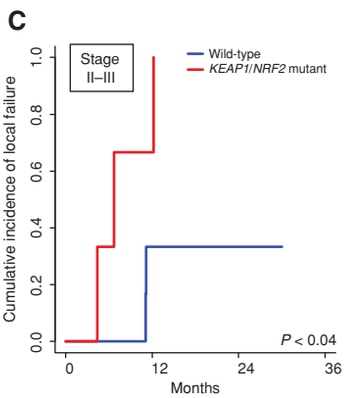

D

Patient	Age	Sex	Stage	*KEAP1* mutations: Tumor variant	*KEAP1* mutations: ctDNA variant (%AF)
T1	56	F	IIIB	M503I	M503I (3.38%)
T2	56	F	IIIB	R483C	R483C (0.44%)
T11	46	F	IIA	Wild-type	Wild-type
T13	81	F	IB	Wild-type	Wild-type
T14	78	M	IB	Wild-type	Wild-type
T23	51	F	IIIA	Wild-type	Wild-type
T35	48	F	IIIB	Wild-type	Wild-type

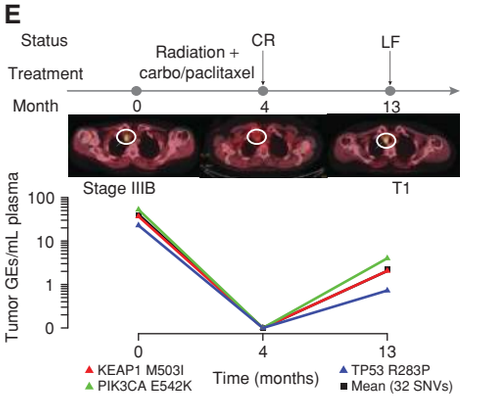

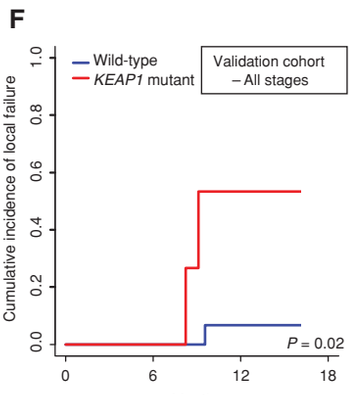

Figure 7. *KEAP1/NRF2* mutation status predicts local failure after radiotherapy in human NSCLC. **A,** Clinical characteristics of a cohort of patients with stage I–III NSCLC treated with curative intent RT and analyzed for *KEAP1/NRF2* mutation status using targeted next-generation sequencing. **B** and **C,** Association of *KEAP1/NRF2* mutations with local failure in patients with NSCLC treated with RT. **B,** Entire cohort. **C,** Stage II–III patients treated with conventionally fractionated radiotherapy or chemoradiotherapy. **D,** Noninvasive identification of *KEAP1* mutation status in ctDNA isolated from pretreatment plasma samples of 7 patients from the cohort in **A** using CAPP-Seq. **E,** Monitoring of ctDNA in a *KEAP1*-mutant patient from **D** treated with chemoradiation. CR, complete response; LF, local failure; carbo, carboplatin. **F,** Clinical characteristics of a validation cohort of patients with stage I–III NSCLC treated with curative intent RT and analyzed for *KEAP1/NRF2* mutation status using targeted next-generation sequencing.

results suggest that *KEAP1/NRF2* mutation status is a predictor of local recurrence after RT in patients with NSCLC.

DISCUSSION

In this study, we demonstrate that deletion of *Keap1* or *Trp53* in murine ABSCs promotes their self-renewal, leading to expansion of mutant stem cell clones. Furthermore, we show that deletion of *Trp53* with or without *Keap1* leads to LSCC formation and that ABSCs are the cell of origin in these LSCC models. The effects of *Keap1* loss appear to be predominantly mediated by NRF2 activation and subsequent lowering of intracellular ROS, leading to increased tumor proliferation, metastasis, and resistance to oxidative stresses and irradiation. Finally, we show for the first time that *KEAP1/NRF2* mutations strongly predict clinical resistance to RT in patients with NSCLC. Although several prior studies have suggested a role for KEAP1 and NRF2 in radioresistance, none have examined the association of mutations in these genes with radiation resistance. Instead, the prior studies either did not contain clinical data and focused on preclinical experiments (35–37), analyzed other clinical outcomes and not local control (38–40), or analyzed gene expression signatures (41). Because mutation status can be readily established in clinical laboratories using widely available genotyping methods, our findings have potential clinical implications.

In order to study the role of *Trp53* and *Keap1* in ABSC self-renewal *in vivo*, we developed a novel lineage-tracing method specific for ABSCs. Although intranasal Ad-Cre is used routinely to knock out genes in the lung, we found that it is unable to transduce upper airway epithelial cells in homeostatic condition, likely due to the mucociliary barrier. Importantly, these data indicate that previous Ad-Cre–induced lung cancer models have likely not explored central airway basal cells as a potential cell of origin. By combining SO_2 injury (42) and Ad-Cre intranasal instillation, we could efficiently transduce tracheal basal cells of immunocompetent mice and lineage-trace them during regeneration. Our lineage-tracing method is complementary to conventional *Krt5*-driven lineage tracing in airway stem cells. One advantage of our approach is that unlike the former methods, it does not lead to recombination in other *Krt5*-expressing tissues such as the skin or esophagus.

We established LSCC models based on loss of *Trp53* and *Keap1,* which mimic mutations occurring in >80% and >30% of human LSCCs, respectively, and which have not been previously explored in murine LSCC models. We found that the type of lung cancer formed by deletion of *Trp53* is dependent on the normal cell type that is targeted. Specifically, inactivation of *Trp53* by Ad-Cre inhalation, which leads to recombination in peripheral lung cells but not in the central airway, led to $SFTPC^+TTF1^+KRT5^-$ LUAD formation. This finding is consistent with that of previous studies (18, 43, 44), which found that inactivation of *Trp53* induced by Ad-Cre inhalation led only to LUAD formation. However, when we specifically induced deletion of *Trp53* with or without *Keap1* in tracheal epithelial cells, LSCCs were generated.

Our experimental approach allowed us to explore the cell of origin of LSCC using a similar strategy as has been successfully applied in prostate and esophageal cancers (22, 23). However, one drawback of this approach is that we could not induce LSCCs orthotopically in immunocompetent mice due to formation of LUADs when using Ad-Cre or skin tumors when using mice with $Krt5^{CreERT2}$, both with a latency of ~2 months. This suggests that LSCCs may have a relatively long latency in mice. In support of this notion, time to tumor formation in previously published LSCC models has been reported to be ~8 to 10 months (2, 19, 20). Additionally, our use of immunodeficient mice makes our approach suboptimal for studies on tumor immunology and immunotherapy. However, we believe that our model, using either subcutaneous or orthotopic transplantation, will be useful for studies focused on other aspects of cancer biology, including tumor initiation, metastasis, and treatment resistance.

We found that only tracheal ABSCs and not more differentiated tracheal luminal cells, which contain secretory and ciliated cells, could form LSCCs, indicating that ABSCs are the cell of origin in our model. Interestingly, a recent study showed that $Scgb1a1^+$ secretory cells can dedifferentiate into ABSCs (45), raising the question of why luminal cells could not give rise to tumors in our model. One potential explanation for this is that the process of dedifferentiation may not function properly in the presence of the gene expression changes induced by loss of *Trp53* with or without loss of *Keap1*. Another possible explanation is that, although basal cells arising from secretory cells are able to self-renew and repair tissue upon injury, they may not be entirely identical to basal cells at homeostasis and may differ in ability to undergo tumorigenesis. Lastly, considering the importance of stem cell and stromal interaction, the transplanted microenvironment may not favor dedifferentiation.

Nonetheless, our results are consistent with findings from other LSCC models. For example, in a recent study (3), Xiao and colleagues provided data indicating that *IKKα* inactivation in KRT5-expressing lung cells, but not other types of lung cells, leads to LSCC formation, consistent with our findings of ABSCs as the cell of origin in our LSCC models. Separately, in an *Lkb1;Pten* deletion–based LSCC model, SPC-Cre and CCSP-Cre failed to produce tumors, and endotracheal Ad-Cre administration led to only LSCC formation (2). This indicates that alveolar type II pneumocytes and club cells are not the cell of origin in this model and suggests that another cell type, possibly rare KRT5-expressing peribronchiolar cells (46), is the source of these tumors.

However, other data suggest that murine LSCCs do not originate only from ABSCs. Rather, a complex interplay between the cell of origin and the driver mutation appears to determine the type of lung cancer that develops. For example, recent studies revealed that *Kras* activated/*Lkb1*-deficient LUADs, which originated from type II pneumocytes, can transdifferentiate into LSCC (47–49). Also, CCSP-Cre induced SOX2 overexpression, and *Kras* activation can lead to squamous hyperplasia (50). Additionally, some data suggest that KRT5-expressing cells may be able to give rise to LUADs. Specifically, $Krt5^{CrePR}$-mediated *Kras* activation or *Pten* deletion resulted in mixed LSCC and LUAD tumors, although as the authors point out, this may have been due to leakiness of the promoter that was used (51). Thus, it appears that the cell of origin may dictate the lung cancer subtype that forms for certain mutations such as *Trp53* but not for others such as *Kras* and *Sox2*. Interestingly, the cell of origin

appears to determine lung cancer subtype when the driver gene is commonly mutated in both LSCC and LUAD (e.g., *Trp53*). Conversely, driver mutations that are predominantly observed in human LSCC, such as *Sox2* and *Lkb1,* appear to be able to induce LSCC even in bronchiolar club cells or alveolar type II cells, whereas mutations that are predominantly observed in human LUADs, such as *Kras,* appear to be able to drive LUAD formation in murine ABSCs. Thus, at least in the mouse, lung cancer subtypes appear to be determined by the interplay of cell type and genotype.

Our results suggest a critical role for mutations in *TP53* and *KEAP1* during LSCC oncogenesis, because deletion of either gene leads to increased self-renewal of ABSCs. Significantly, the impact of *Trp53* loss on ABSC self-renewal and the fact that loss of both *Trp53* and *Keap1* leads to increased self-renewal compared with loss of either gene alone have not been previously demonstrated and are of clinical relevance, because *TP53* is mutated in over 80% of human LSCCs harboring *KEAP1* mutations (5). Congruent with our findings, Paul and colleagues recently also reported a role for ROS regulation in ABSC homeostasis that was mediated through increased Notch pathway signaling and reflected by gene expression changes of Notch pathway components upon NRF2 modulation (16). We did not observe any differences in expression of the same genes by *Keap1* deletion, suggesting that this Notch-based mechanism does not play a major role in mediating the effects of NRF2 activation in our LSCC models.

Our findings suggest that once an ABSC acquires mutations in either *TP53* or *KEAP1*, it will be able to outcompete WT stem cells, thus creating an expanding pool of mutated cells that are at risk for acquiring additional genetic hits and ultimately leading to LSCC formation. Indeed, evidence consistent with such clonal expansion of mutant ABSCs has been demonstrated in humans. Specifically, it has been shown that preinvasive lesions consisting of keratin 14–expressing basal cells that contain *TP53* mutations can expand through large portions of the bronchial tree, including spreading from one side to the other (52, 53). Although the mutation status of *KEAP1* has not been examined in these studies, we speculate that a premalignant clone containing a *TP53* mutation would gain significant additional fitness if it acquired mutations in *KEAP1*, mediated by the increased proliferation, migration, and resistance to oxidative stress that we observed in our model.

From a clinical standpoint, our finding of most immediate potential impact is the observation that *KEAP1/NRF2* mutation status predicts the rate of local failure after radiotherapy in patients with NSCLC. Because radiotherapy kills cells by induction of ROS that lead to DNA double-strand breaks, *KEAP1/NRF2*-mutant tumors are likely resistant to RT due to enhanced expression of ROS scavengers and detoxification pathways. However, we cannot rule out that additional somatic or epigenetic alterations that we did not interrogate may play a role in the higher incidence of local recurrence in *KEAP1/NRF2*-mutant tumors. Thus, future studies should include human models with more complex genetics and examine the effects of *KEAP1* loss in *TP53* WT tumors in order to further explore the role of *KEAP1/NRF2* in radiation resistance.

KEAP1/NRF2 mutation status was not associated with overall survival in our cohorts or in the LUAD (54) and LSCC (5) cohorts from TCGA (data not shown). However, Kim and colleagues previously found that *NRF2* mutations were statistically significantly associated with worse overall survival in LSCC (55). We hypothesize that these conflicting results likely relate to statistical power, differences in clinical covariates among the different cohorts, and the potential impact of additional somatic or epigenetic modifiers of tumor aggressiveness whose prevalence may differ between studies.

All of the *KEAP1* mutations we identified in human patients were somatic and appeared to be heterozygous. This observation is consistent with prior studies that have shown that mutation of *KEAP1* on both alleles is not required to achieve functional effects. For example, mutant KEAP1 proteins can form heterodimers with WT proteins and function as dominant-negatives, inhibiting the association with NRF2 (56, 57). Separately, epigenetic modifications of *KEAP1* promoter associated with loss of expression have been reported in a variety of malignancies, including lung cancer (58–60).

Our observation of *KEAP1/NRF2* mutations in the plasma of patients with NSCLC being treated with RT suggests that noninvasive mutation assessment using ctDNA could be a valuable approach for facilitating personalized management of patients with NSCLC who have limited tissue samples available for molecular analysis. Given the high rate of local failure we observed in patients with *KEAP1/NRF2* mutations, mutation testing for these genes in tumor or plasma could potentially be used to personalize treatment strategies for patients with NSCLC. Although personalized medicine approaches based on mutation testing are routinely used to identify the most appropriate systemic therapy in advanced NSCLC, similar approaches are not being used to select treatments for patients with localized NSCLC. We speculate that *KEAP1/NRF2* mutation status could potentially be used to select the best choice of local therapy for such patients or to identify patients who might benefit from radiation dose escalation. Furthermore, inhibition of critical NRF2 targets, such as system x_c^-, may allow targeted radiosensitization in patients with *KEAP1/NRF2* mutations. Prospective studies to validate the association of *KEAP1/NRF2* mutations with radioresistance and to test personalized treatment approaches will, of course, be critical. Lastly, because *KEAP1/NRF2* mutations are found in many other cancer types (61–65), we hypothesize that they may contribute to radioresistance in a substantial fraction of patients. Therefore, strategies for countering NRF2 activation may improve personalized therapy and outcomes for a large number of patients with cancer.

METHODS

Mouse Tracheal Epithelial Cell Isolation and FACS

Mouse tracheae were harvested and incubated in dispase (Invitrogen; #17105-041) for 40 minutes at 37°C and longitudinally opened. The epithelium was peeled off and incubated in 0.25% trypsin for 5 minutes at 37°C. Trypsinized epithelium was centrifuged, treated with ammonium–chloride–potassium (ACK) lysis buffer to lyse the red blood cells, and filtered through a 40-μm cell strainer (BD Biosciences). After centrifugation, cells were resuspended in blocking buffer (Hank's Balanced Salt Solution with 2% bovine calf serum) and stained with anti-mouse CD31, CD45, CD140a, CD49f, and

CD326 (Biolegend; antibody lists are in Supplementary Table S4). Cells were sorted using the BD FACS Aria.

Mouse Tracheosphere Culture and Passaging

Primary tracheal epithelial cells were resuspended in MTEC/Plus (66) mixed at a 1:1 ratio with growth factor–reduced Matrigel (67). Cell/media/matrigel mixture (100 μL) was plated on top of a 24-well cell culture insert for air–liquid interface culture. Media (0.4 mL) were provided to the lower chamber and changed every other day. Sphere formation and growth were followed for at least 10 to 14 days. Spheres (>50 μm in diameter) were counted manually. For the secondary sphere formation assay, spheres were dissociated with dispase for 40 minutes, digested with trypsin/0.05% EDTA for 5 minutes, and passaged through a 27-G needle five times to dissociate into single cells (68). After centrifugation, cells were resuspended and filtered through a 40-μm cell strainer for further analysis or culture. The same number of tdTomoto$^+$ cells was FACS-sorted and cultured for the secondary tracheosphere culture.

Mouse Studies

Keap1$^{+/f}$ mice (C57BL/6J background) were a kind gift from T. Kensler (University of Pittsburgh, PA; refs. 69, 70). *Trp53*$^{+/f}$; *R26*^{tdTomato} mice (B6/129 background) were a kind gift from M. Winslow (Stanford University, CA; ref. 71). Mouse cohorts of WT *R26*^{tdTomato}, *Keap1*$^{f/f}$;*R26*^{tdTomato}, *Trp53*$^{f/f}$;*R26*^{tdTomato}, and *Keap1*$^{f/f}$; *Trp53*$^{f/f}$;*R26*^{tdTomato} were generated by mating *Keap1*$^{+/f}$ mice and *Trp53*$^{+/f}$;*R26*^{tdTomato} mice. NSG mice, *Krt5*^{CreERT2} mice, and nude mice were obtained from The Jackson Laboratory and Charles River Laboratories. All mice were genotyped by previously reported methods (69, 71, 72), and mice between 4 weeks and 9 months of age were used for experiments. The LSCC was established by implanting *in vitro* or *in vivo* recombined tracheal cells or tumor cells into NSG mice. Mice were housed in a designated pathogen-free area in a facility at the Stanford University School of Medicine accredited by the Association for the Assessment and Accreditation of Laboratory Animal Care. All care and treatment of experimental animals were in accordance with Stanford University School of Medicine institutional animal care and use committee guidelines. For SO_2 injury, adult mice were exposed to 500 ppm SO_2 in air for 5 hours (73). After 18 to 24 hours, Ad-Cre viruses were intranasally inhaled into mouse lung. For *in vivo* recombination for the cell-of-origin experiments, 250 mg/g tamoxifen was intraperitoneally injected into *Krt5*^{CreERT2};*Keap1*$^{f/f}$;*Trp53*$^{f/f}$;*R26*^{tdTomato} mice. After ~4 months, recombined basal and luminal cells were sorted and subcutaneously transplanted into NSG mice for tumor generation.

Generation and Establishment of Lung Tumors

For *de novo* murine tumor generation, 10k to 30k tracheal epithelial cells from WT *R26*^{tdTomato}, *Keap1*$^{f/f}$;*R26*^{tdTomato}, *Trp53*$^{f/f}$;*R26*^{tdTomato}, and *Keap1*$^{f/f}$; *Trp53*$^{f/f}$;*R26*^{tdTomato} mice were harvested and transduced by Ad-Cre viruses *in vitro* overnight at 37°C. The next day, cells were resuspended in 200 μL of a 1:1 mixture of the culture medium and Matrigel and subcutaneously transplanted into NSG mice. For tumor growth assays, primary lung tumor cells were suspended in a 1:1 mixture of the culture medium and Matrigel and were subcutaneously injected into nude mice. Tumor sizes were measured every 2 to 3 days after tumor inoculation and continued throughout the experiment. Tumor volumes were calculated using the formula (length × width^2)/2. To analyze the effect of irradiation on tumor growth, when tumor volumes reached ~100 mm^3, mice were randomly divided into two groups, and irradiation was focally delivered. Tumor volumes were measured every other day. Mice displaying severe radiation toxicity (i.e., dramatic weight loss within ~3 days after irradiation attributed to inadequate shielding) were excluded from the analysis.

Tumor Dissociation and Flow Cytometry

Tumors generated from *Trp53*- or *Keap1*;*Trp53*-null tracheal cells were minced with a razor blade and suspended in 10 mL of L-15 Leibovitz medium (Thermo Fisher Scientific Inc.) supplemented with 0.5 mL of collagenase/hyaluronidase (Stem Cell Technologies). Tumors were digested for 1.5 to 2 hours at 37°C and 5% CO_2 with manual dissociation by pipetting every 30 minutes. Once digested, 40 mL of blocking buffer was added and tumor cells were collected by centrifugation. Tumor cells were resuspended in 5 mL of trypsin/0.05% EDTA for 5 minutes and centrifuged with the addition of blocking buffer. The cell pellet was incubated with 100 Kunitz units of DNase I (Sigma) and Dispase (Stem Cell Technologies) for 5 minutes at 37°C and centrifuged again with the addition of blocking buffer. Once digested, tumor cells were treated with ACK lysis buffer and filtered through a 40-μm cell strainer. After centrifugation, tumor cells were resuspended in blocking buffer, blocked with rat IgG for 10 minutes, and stained with rat anti-mouse CD31, CD45, and SCA1, and rat anti-human/mouse CD49f. CD31- and CD45-negative viable cells with strong red signal were sorted for further analysis.

Metastasis Model

Tumor cells (2,000–5,000) were injected into NSG mice via the tail vein after preincubation with PBS or N-acetylcysteine (NAC) for 2 hours. The detailed information is described in Supplementary Methods.

Cell Invasion Assay

Tumor cell invasion assays were performed according to the manufacturer's instruction (Trevigen; see Supplementary Methods).

Histology and Immunostaining

Tissues or spheres grown in Matrigel were embedded in OCT compound (Sakura) and immediately frozen on dry ice for frozen section or fixed in 4% paraformaldehyde overnight, transferred to 70% ethanol, and embedded in paraffin. The detailed information is described in Supplementary Methods.

γ-H2AX Detection

Thirty minutes after irradiation, irradiated and nonirradiated cells were fixed in ice-cold 50% ethanol and 50% methanol for 20 minutes for γ-H2AX foci evaluation. The detailed information is described in Supplementary Methods.

Human NSCLC Cohorts

We analyzed tumor specimens from patients undergoing definitive treatment for newly diagnosed NSCLC who were enrolled in a study approved by the Stanford University Institutional Review Board and who had provided informed consent in accordance with the Declaration of Helsinki. All patients analyzed had biopsy-confirmed primary NSCLC, stage IA–IIIB according to the seventh edition American Joint Committee on Cancer staging manual. Patients who underwent surgery were excluded. Patients with stage I NSCLC were treated with stereotactic ablative radiotherapy (SABR), whereas patients with stage II–III NSCLC were treated with conventionally fractionated radiotherapy or concurrent chemoradiotherapy. Local failure was defined as previously described (74). For the initial cohort, tissue blocks were obtained and clinical outcomes were collected from patient records. A subset of these patients also donated blood samples for biomarker analysis. For the independent validation cohort, plasma samples were collected prior to treatment.

Detection of KEAP1 Variants in Tumor Specimens and ctDNA

Tumor genotyping was performed using a hybrid capture-based approach on formalin-fixed, paraffin-embedded tumor samples to determine *KEAP1*, *NRF2*, and *TP53* mutation status, as previously described (33). Matched germline was also sequenced when available. Briefly, single-nucleotide variants (SNV) were called using an in-house

pipeline for processing targeted sequencing data that used BWA sampe 0.5.9-r16 and SAMtools mpileup 0.1.18-r579. The GRCh37/hg19 reference genome was used. Only properly paired reads and bases with a phred quality score of at least 30 were considered, and base alignment quality adjustment (BAQ) was enabled for calling SNVs. When matched germline was available, variants at ≥2.5% were called, and when only tumor DNA was available, variants at ≥5% were called.

For ctDNA analyses, CAPP-Seq was performed on cell-free DNA isolated from plasma samples as recently described (34). Briefly, cell-free DNA was isolated, and sequencing libraries were prepared using adapters containing molecular barcodes. To further reduce sequencing errors, data were background-polished. Noninvasive genotyping was performed to call nonsynonymous SNVs and indels in *KEAP1*, *NRF2*, and *TP53* that were present in pretreatment plasma but not matched germline DNA obtained from plasma-depleted whole blood. For one patient, plasma samples were also available immediately posttreatment and at the time of local recurrence. The global amount of ctDNA in each sample was calculated using SNVs and indel reporters detected in the tumor biopsy.

RNA-seq Library Preparation, Sequencing, and Gene Expression Analysis

The detailed information from RNA isolation of FACS-sorted cells to RNA-seq analysis is described in Supplementary Methods.

Generation of Lentiviral Supernatants and Infection of Primary Lung Cancer Cells

sh*Nrf2* expression plasmids were purchased from OriGene (TL515053). Lentiviral generation and transduction of primary lung cancer cells were described in Supplementary Methods.

Real-Time RT-PCR

RNA from primary sorted cells was isolated using the RNeasy Micro Kit (Qiagen), and cDNA was prepared using the High-Capacity cDNA Reverse Transcription Kit (ABI). The detailed information is described in Supplementary Methods.

Statistical Analyses

Statistical analyses were performed using unpaired two-sided Student t test between groups at each time point after checking that variances were similar between groups, and significance was defined based on $P < 0.05$. Data are presented as mean ± SEM of 3 or more independent biological replicates. Competing risk analyses were performed in the R statistical program, and Gray's tests were used to compare strata. Sample numbers were determined empirically using estimation of sample size considering the variation and mean of the samples. For animal experiments, this ranged from 4 to 10 animals per group. No statistical method was used to predetermine sample size. Animals were randomly assigned to groups for *in vivo* studies. Assessment was performed without blinding.

Disclosure of Potential Conflicts of Interest

A. Lovejoy is a senior scientist at Roche. A.M. Newman has ownership interest (including patents) in Capp Medical, Inc., and is a consultant/advisory board member for Roche. B.W. Loo is a board member at TibaRay, Inc., reports receiving commercial research grants from Varian Medical Systems and RaySearch Laboratories, and has ownership interest (including patents) in TibaRay, Inc. M. Diehn is a consultant/advisory board member for Roche. No potential conflicts of interest were disclosed by the other authors.

Authors' Contributions

Conception and design: Y. Jeong, A.A. Alizadeh, M. Diehn
Development of methodology: Y. Jeong, W. Kong, R.B. West, P. Beachy, A.A. Alizadeh, M. Diehn
Acquisition of data (provided animals, acquired and managed patients, provided facilities, etc.): Y. Jeong, N.T. Hoang, A. Lovejoy, D. Truong, S. Martin, D. Heiser, L. Zhou, C. Say, J.N. Carter, S.M. Hiniker, B.W. Loo Jr, R.B. West, A.A. Alizadeh, M. Diehn
Analysis and interpretation of data (e.g., statistical analysis, biostatistics, computational analysis): Y. Jeong, N.T. Hoang, A. Lovejoy, H. Stehr, A.M. Newman, A.J. Gentles, A. Chaudhuri, S.M. Hiniker, A.A. Alizadeh, M. Diehn
Writing, review, and/or revision of the manuscript: Y. Jeong, N.T. Hoang, A. Lovejoy, H. Stehr, A.J. Gentles, S.M. Hiniker, B.W. Loo Jr, R.B. West, P. Beachy, A.A. Alizadeh, M. Diehn
Administrative, technical, or material support (i.e., reporting or organizing data, constructing databases): Y. Jeong, H. Stehr, A. Chaudhuri, L. Zhou, J.N. Carter, S.M. Hiniker, M. Diehn
Study supervision: Y. Jeong, A.A. Alizadeh, M. Diehn
Other (SO2 injury): W. Kong
Other (provided injury system): P. Beachy

Acknowledgments

We thank J. Sage, A. Sweet-Cordero, M. Winslow (Stanford University), T. Kensler (University of Pittsburgh), and members of their labs for supplying reagents and suggestions. We also thank R. von Eyben for statistical advice.

Grant Support

This work was supported by grants from the California Institute for Regenerative Medicine (TG2-01159, Y. Jeong; TB1-01194, N.T. Hoang), the NIH (P30CA147933 and P01CA139490, M. Diehn; R01CA188298, A.A. Alizadeh and M. Diehn), the V Foundation (V Scholar Award, M. Diehn), the CRK Faculty Scholar Fund (M. Diehn), and the Virginia and D.K. Ludwig Foundation (M. Diehn). M. Diehn was also supported by a Doris Duke Clinical Scientist Development Award and an NIH New Innovator Award (1-DP2-CA186569).

The costs of publication of this article were defrayed in part by the payment of page charges. This article must therefore be hereby marked *advertisement* in accordance with 18 U.S.C. Section 1734 solely to indicate this fact.

Received January 28, 2016; revised September 20, 2016; accepted September 22, 2016; published OnlineFirst September 23, 2016.

REFERENCES

1. Cancer.org [Internet]. Atlanta: American Cancer Society. Cancer Facts & Figures 2014; c2016. Available from: http://www.cancer.org/research/cancerfactsstatistics/cancerfactsfigures2014/
2. Xu C, Fillmore CM, Koyama S, Wu H, Zhao Y, Chen Z, et al. Loss of Lkb1 and Pten leads to lung squamous cell carcinoma with elevated PD-L1 expression. Cancer Cell 2014;25:590–604.
3. Xiao Z, Jiang Q, Willette-Brown J, Xi S, Zhu F, Burkett S, et al. The pivotal role of IKKalpha in the development of spontaneous lung squamous cell carcinomas. Cancer Cell 2013;23:527–40.
4. Mukhopadhyay A, Berrett KC, Kc U, Clair PM, Pop SM, Carr SR, et al. Sox2 cooperates with Lkb1 loss in a mouse model of squamous cell lung cancer. Cell Rep 2014;8:40–9.
5. Cancer Genome Atlas Research N. Comprehensive genomic characterization of squamous cell lung cancers. Nature 2012;489:519–25.
6. Itoh K, Chiba T, Takahashi S, Ishii T, Igarashi K, Katoh Y, et al. An Nrf2/small Maf heterodimer mediates the induction of phase II detoxifying enzyme genes through antioxidant response elements. Biochem Biophys Res Commun 1997;236:313–22.
7. Itoh K, Wakabayashi N, Katoh Y, Ishii T, Igarashi K, Engel JD, et al. Keap1 represses nuclear activation of antioxidant responsive elements by Nrf2 through binding to the amino-terminal Neh2 domain. Genes Dev 1999;13:76–86.
8. Kobayashi A, Kang MI, Okawa H, Ohtsuji M, Zenke Y, Chiba T, et al. Oxidative stress sensor Keap1 functions as an adaptor for Cul3-based

E3 ligase to regulate proteasomal degradation of Nrf2. Mol Cell Biol 2004;24:7130–9.
9. DeNicola GM, Karreth FA, Humpton TJ, Gopinathan A, Wei C, Frese K, et al. Oncogene-induced Nrf2 transcription promotes ROS detoxification and tumorigenesis. Nature 2011;475:106–9.
10. Satoh H, Moriguchi T, Takai J, Ebina M, Yamamoto M. Nrf2 prevents initiation but accelerates progression through the Kras signaling pathway during lung carcinogenesis. Cancer Res 2013;73:4158–68.
11. Yamadori T, Ishii Y, Homma S, Morishima Y, Kurishima K, Itoh K, et al. Molecular mechanisms for the regulation of Nrf2-mediated cell proliferation in non-small-cell lung cancers. Oncogene 2012;31:4768–77.
12. Sayin VI, Ibrahim MX, Larsson E, Nilsson JA, Lindahl P, Bergo MO. Antioxidants accelerate lung cancer progression in mice. Sci Transl Med 2014;6:221ra15.
13. Le Gal K, Ibrahim MX, Wiel C, Sayin VI, Akula MK, Karlsson C, et al. Antioxidants can increase melanoma metastasis in mice. Sci Transl Med 2015;7:308re8.
14. Bauer AK, Hill T 3rd, Alexander CM. The involvement of NRF2 in lung cancer. Oxid Med Cell Longev 2013;2013:746432.
15. Rock JR, Randell SH, Hogan BL. Airway basal stem cells: a perspective on their roles in epithelial homeostasis and remodeling. Dis Model Mech 2010;3:545–56.
16. Paul MK, Bisht B, Darmawan DO, Chiou R, Ha VL, Wallace WD, et al. Dynamic changes in intracellular ROS levels regulate airway basal stem cell homeostasis through Nrf2-dependent Notch signaling. Cell Stem Cell 2014;15:199–214.
17. DuPage M, Dooley AL, Jacks T. Conditional mouse lung cancer models using adenoviral or lentiviral delivery of Cre recombinase. Nat Protoc 2009;4:1064–72.
18. Meuwissen R, Linn SC, Linnoila RI, Zevenhoven J, Mooi WJ, Berns A. Induction of small cell lung cancer by somatic inactivation of both Trp53 and Rb1 in a conditional mouse model. Cancer Cell 2003;4:181–9.
19. Wang Y, Zhang Z, Yan Y, Lemon WJ, LaRegina M, Morrison C, et al. A chemically induced model for squamous cell carcinoma of the lung in mice: histopathology and strain susceptibility. Cancer Res 2004;64:1647–54.
20. Lijinsky W, Reuber MD. Neoplasms of the skin and other organs observed in Swiss mice treated with nitrosoalkylureas. J Cancer Res Clin Oncol 1988;114:245–9.
21. Lee JH, Bhang DH, Beede A, Huang TL, Stripp BR, Bloch KD, et al. Lung stem cell differentiation in mice directed by endothelial cells via a BMP4-NFATc1-thrombospondin-1 axis. Cell 2014;156:440–55.
22. Goldstein AS, Huang J, Guo C, Garraway IP, Witte ON. Identification of a cell of origin for human prostate cancer. Science 2010;329:568–71.
23. Liu K, Jiang M, Lu Y, Chen H, Sun J, Wu S, et al. Sox2 cooperates with inflammation-mediated Stat3 activation in the malignant transformation of foregut basal progenitor cells. Cell Stem Cell 2013;12:304–15.
24. Subramanian A, Tamayo P, Mootha VK, Mukherjee S, Ebert BL, Gillette MA, et al. Gene set enrichment analysis: a knowledge-based approach for interpreting genome-wide expression profiles. Proc Natl Acad Sci U S A 2005;102:15545–50.
25. Thu KL, Pikor LA, Chari R, Wilson IM, Macaulay CE, English JC, et al. Genetic disruption of KEAP1/CUL3 E3 ubiquitin ligase complex components is a key mechanism of NF-kappaB pathway activation in lung cancer. J Thorac Oncol 2011;6:1521–9.
26. Lee DF, Kuo HP, Liu M, Chou CK, Xia W, Du Y, et al. KEAP1 E3 ligase-mediated downregulation of NF-kappaB signaling by targeting IKKbeta. Mol Cell 2009;36:131–40.
27. Hall EJ, Giaccia AJ. Radiobiology for the radiologist. 7th ed. Philadelphia: Lippincottt Williams & Wilkins; 2011.
28. Lo M, Wang YZ, Gout PW. The x(c)-cystine/glutamate antiporter: a potential target for therapy of cancer and other diseases. J Cell Physiol 2008;215:593–602.
29. Huang Y, Dai Z, Barbacioru C, Sadee W. Cystine-glutamate transporter SLC7A11 in cancer chemosensitivity and chemoresistance. Cancer Res 2005;65:7446–54.
30. Yoshikawa M, Tsuchihashi K, Ishimoto T, Yae T, Motohara T, Sugihara E, et al. xCT inhibition depletes CD44v-expressing tumor cells that are resistant to EGFR-targeted therapy in head and neck squamous cell carcinoma. Cancer Res 2013;73:1855–66.
31. Ma MZ, Chen G, Wang P, Lu WH, Zhu CF, Song M, et al. Xc- inhibitor sulfasalazine sensitizes colorectal cancer to cisplatin by a GSH-dependent mechanism. Cancer Lett 2015;368:88–96.
32. Thunnissen E, Kerr KM, Herth FJ, Lantuejoul S, Papotti M, Rintoul RC, et al. The challenge of NSCLC diagnosis and predictive analysis on small samples. Practical approach of a working group. Lung Cancer 2012;76:1–18.
33. Newman AM, Bratman SV, To J, Wynne JF, Eclov NC, Modlin LA, et al. An ultrasensitive method for quantitating circulating tumor DNA with broad patient coverage. Nat Med 2014;20:548–54.
34. Newman AM, Lovejoy AF, Klass DM, Kurtz DM, Chabon JJ, Scherer F, et al. Integrated digital error suppression for improved detection of circulating tumor DNA. Nat Biotechnol 2016;34:547–55.
35. Abazeed ME, Adams DJ, Hurov KE, Tamayo P, Creighton CJ, Sonkin D, et al. Integrative radiogenomic profiling of squamous cell lung cancer. Cancer Res 2013;73:6289–98.
36. Lee S, Lim MJ, Kim MH, Yu CH, Yun YS, Ahn J, et al. An effective strategy for increasing the radiosensitivity of Human lung Cancer cells by blocking Nrf2-dependent antioxidant responses. Free Radic Biol Med 2012;53:807–16.
37. Singh A, Bodas M, Wakabayashi N, Bunz F, Biswal S. Gain of Nrf2 function in non-small-cell lung cancer cells confers radioresistance. Antioxid Redox Signaling 2010;13:1627–37.
38. Cescon DW, She D, Sakashita S, Zhu CQ, Pintilie M, Shepherd FA, et al. NRF2 pathway activation and adjuvant chemotherapy benefit in lung squamous cell carcinoma. Clin Cancer Res 2015;21:2499–505.
39. Solis LM, Behrens C, Dong W, Suraokar M, Ozburn NC, Moran CA, et al. Nrf2 and Keap1 abnormalities in non–small cell lung carcinoma and association with clinicopathologic features. Clin Cancer Res 2010;16:3743–53.
40. Shibata T, Ohta T, Tong KI, Kokubu A, Odogawa R, Tsuta K, et al. Cancer related mutations in NRF2 impair its recognition by Keap1–Cul3 E3 ligase and promote malignancy. Proc Natl Acad Sci U S A 2008;105:13568–73.
41. Shibata T, Kokubu A, Saito S, Narisawa-Saito M, Sasaki H, Aoyagi K, et al. NRF2 mutation confers malignant potential and resistance to chemoradiation therapy in advanced esophageal squamous cancer. Neoplasia 2011;13:864–73.
42. Borthwick DW, Shahbazian M, Krantz QT, Dorin JR, Randell SH. Evidence for stem-cell niches in the tracheal epithelium. Am J Respir Cell Mol Biol 2001;24:662–70.
43. Jackson EL, Olive KP, Tuveson DA, Bronson R, Crowley D, Brown M, et al. The differential effects of mutant p53 alleles on advanced murine lung cancer. Cancer Res 2005;65:10280–8.
44. Sutherland KD, Proost N, Brouns I, Adriaensen D, Song JY, Berns A. Cell of origin of small cell lung cancer: inactivation of Trp53 and Rb1 in distinct cell types of adult mouse lung. Cancer Cell 2011;19:754–64.
45. Tata PR, Mou H, Pardo-Saganta A, Zhao R, Prabhu M, Law BM, et al. Dedifferentiation of committed epithelial cells into stem cells in vivo. Nature 2013;503:218–23.
46. Zuo W, Zhang T, Wu DZ, Guan SP, Liew AA, Yamamoto Y, et al. p63(+)Krt5(+) distal airway stem cells are essential for lung regeneration. Nature 2015;517:616–20.
47. Gao Y, Zhang W, Han X, Li F, Wang X, Wang R, et al. YAP inhibits squamous transdifferentiation of Lkb1-deficient lung adenocarcinoma through ZEB2-dependent DNp63 repression. Nat Commun 2014;5:4629.
48. Han X, Li F, Fang Z, Gao Y, Li F, Fang R, et al. Transdifferentiation of lung adenocarcinoma in mice with Lkb1 deficiency to squamous cell carcinoma. Nat Commun 2014;5:3261.
49. Li F, Han X, Li F, Wang R, Wang H, Gao Y, et al. LKB1 inactivation elicits a redox imbalance to modulate non–small cell lung cancer plasticity and therapeutic response. Cancer Cell 2015;27:698–711.
50. Xu X, Huang L, Futtner C, Schwab B, Rampersad RR, Lu Y, et al. The cell of origin and subtype of K-Ras-induced lung tumors are modified by Notch and Sox2. Genes Dev 2014;28:1929–39.

51. Malkoski SP, Cleaver TG, Thompson JJ, Sutton WP, Haeger SM, Rodriguez KJ, et al. Role of PTEN in basal cell derived lung carcinogenesis. Mol Carcinog 2014;53:841–6.
52. Franklin WA, Gazdar AF, Haney J, Wistuba II, La Rosa FG, Kennedy T, et al. Widely dispersed p53 mutation in respiratory epithelium. A novel mechanism for field carcinogenesis. J Clin Invest 1997; 100:2133–7.
53. Pipinikas CP, Kiropoulos TS, Teixeira VH, Brown JM, Varanou A, Falzon M, et al. Cell migration leads to spatially distinct but clonally related airway cancer precursors. Thorax 2014;69:548–57.
54. Cancer Genome Atlas Research N. Comprehensive molecular profiling of lung adenocarcinoma. Nature 2014;511:543–50.
55. Kim Y, Hammerman PS, Kim J, Yoon JA, Lee Y, Sun JM, et al. Integrative and comparative genomic analysis of lung squamous cell carcinomas in East Asian patients. J Clin Oncol 2014;32:121–8.
56. Ohta T, Iijima K, Miyamoto M, Nakahara I, Tanaka H, Ohtsuji M, et al. Loss of Keap1 function activates Nrf2 and provides advantages for lung cancer cell growth. Cancer Res 2008;68:1303–9.
57. Suzuki T, Maher J, Yamamoto M. Select heterozygous Keap1 mutations have a dominant-negative effect on wild-type Keap1 in vivo. Cancer Res 2011;71:1700–9.
58. Wang R, An J, Ji F, Jiao H, Sun H, Zhou D. Hypermethylation of the Keap1 gene in human lung cancer cell lines and lung cancer tissues. Biochem Biophys Res Commun 2008;373:151–4.
59. Zhang P, Singh A, Yegnasubramanian S, Esopi D, Kombairaju P, Bodas M, et al. Loss of Kelch-like ECH-associated protein 1 function in prostate cancer cells causes chemoresistance and radioresistance and promotes tumor growth. Mol Cancer Ther 2010;9: 336–46.
60. Muscarella LA, Parrella P, D'Alessandro V, la Torre A, Barbano R, Fontana A, et al. Frequent epigenetics inactivation of KEAP1 gene in non-small cell lung cancer. Epigenetics 2011;6:710–9.
61. Gao YB, Chen ZL, Li JG, Hu XD, Shi XJ, Sun ZM, et al. Genetic landscape of esophageal squamous cell carcinoma. Nat Genet 2014;46:1097–102.
62. Lin DC, Hao JJ, Nagata Y, Xu L, Shang L, Meng X, et al. Genomic and molecular characterization of esophageal squamous cell carcinoma. Nat Genet 2014;46:467–73.
63. Cancer Genome Atlas N. Comprehensive genomic characterization of head and neck squamous cell carcinomas. Nature 2015;517:576–82.
64. Ojesina AI, Lichtenstein L, Freeman SS, Pedamallu CS, Imaz-Rosshandler I, Pugh TJ, et al. Landscape of genomic alterations in cervical carcinomas. Nature 2014;506:371–5.
65. Cancer Genome Atlas Research N. Comprehensive molecular characterization of urothelial bladder carcinoma. Nature 2014;507:315–22.
66. You Y, Richer EJ, Huang T, Brody SL. Growth and differentiation of mouse tracheal epithelial cells: selection of a proliferative population. Am J Physiol Lung Cell Mol Physiol 2002;283:L1315–21.
67. Dontu G, Abdallah WM, Foley JM, Jackson KW, Clarke MF, Kawamura MJ, et al. In vitro propagation and transcriptional profiling of human mammary stem/progenitor cells. Genes Dev 2003;17:1253–70.
68. Lukacs RU, Goldstein AS, Lawson DA, Cheng D, Witte ON. Isolation, cultivation and characterization of adult murine prostate stem cells. Nat Protoc 2010;5:702–13.
69. Wakabayashi N, Shin S, Slocum SL, Agoston ES, Wakabayashi J, Kwak MK, et al. Regulation of notch1 signaling by nrf2: implications for tissue regeneration. Sci Signal 2010;3:ra52.
70. Okawa H, Motohashi H, Kobayashi A, Aburatani H, Kensler TW, Yamamoto M. Hepatocyte-specific deletion of the keap1 gene activates Nrf2 and confers potent resistance against acute drug toxicity. Biochem Biophys Res Commun 2006;339:79–88.
71. Madisen L, Zwingman TA, Sunkin SM, Oh SW, Zariwala HA, Gu H, et al. A robust and high-throughput Cre reporting and characterization system for the whole mouse brain. Nat Neurosci 2010;13:133–40.
72. Jonkers J, Meuwissen R, van der Gulden H, Peterse H, van der Valk M, Berns A. Synergistic tumor suppressor activity of BRCA2 and p53 in a conditional mouse model for breast cancer. Nat Genet 2001;29:418–25.
73. Rawlins EL, Ostrowski LE, Randell SH, Hogan BL. Lung development and repair: contribution of the ciliated lineage. Proc Natl Acad Sci U S A 2007;104:410–7.
74. Trakul N, Chang CN, Harris J, Chapman C, Rao A, Shen J, et al. Tumor volume-adapted dosing in stereotactic ablative radiotherapy of lung tumors. Int J Radiat Oncol Biol Phys 2012;84:231–7.
75. Schaffer BE, Park KS, Yiu G, Conklin JF, Lin C, Burkhart DL, et al. Loss of p130 accelerates tumor development in a mouse model for human small-cell lung carcinoma. Cancer Res 2010;70:3877–83.